

1 Implementing plant hydraulics in the Community Land Model

2 **Daniel Kennedy¹, Sean Swenson², Keith Oleson², David Lawrence², Rosie Fisher², Pierre
3 Gentine¹**

4 ¹Columbia

5 ²National Center for Atmospheric Research, Table Mesa Drive, Boulder, Colorado, USA

6 **Key Points:**

- 7 • A simplified soil-plant-atmosphere continuum model based on hydraulic theory is
8 implemented in the Community Land Model (version 5).
- 9 • Prognostic leaf water potential replaces soil matric potential as the functional basis
10 for water stress, thus reflecting how the leaf water supply (via the xylem network) and
11 evaporative demand act in concert to determine plant water status and thus stomatal
12 conductance and leaf gas exchange.
- 13 • Prognostic root water potential is used to implement hydraulic root water uptake, re-
14 placing the heuristic soil 'wilting' factor .

Abstract

= enter abstract here =

1 Introduction

Trees face emerging climate change risk globally [Allen *et al.*, 2010; Anderegg *et al.*, 2013a]. Understanding vegetation response is a high priority, both for discerning climate impacts and for modeling feedbacks to the carbon and hydrological cycles. In addition to stress from soil moisture drought, vegetation is susceptible to increasing atmospheric transpiration demand [Restaino *et al.*, 2016; Novick *et al.*, 2016a]. Increases in vapor pressure deficit (VPD) have occurred with warming [Ficklin and Novick, 2017; Seager *et al.*, 2015], and are associated with impacts on vegetation [Williams *et al.*, 2013; McDowell and Allen, 2015]. Significant uncertainty remains regarding how vegetation will respond to changes in hydroclimate within Earth System Models, feeding back onto the carbon cycle as vegetation mediates carbon uptake from continents [De Kauwe *et al.*, 2017; Friedlingstein *et al.*, 2014].

Plant water stress parameterizations are important in Earth System Models, as they define vegetation regulation of surface fluxes (photosynthesis, transpiration) to water fluctuations. Vegetation water use strategies also modulate carbon uptake, creating a critical coupling between the Earth System's carbon and hydrological cycles [Green *et al.*, 2017]. Drought stress parameterizations (functions which relate simple metric of soil moisture status to leaf gas exchange) are widely used to define the response of stomatal conductance to vegetation water status that is used to attenuate transpiration, photosynthesis, and root water uptake with drying. The dynamics of water stress in models have broad effects on critical land surface processes [Joetjer *et al.*, 2014]. On diurnal timescales, drought parameterizations influence the partitioning of latent versus sensible heat with effects on surface temperature [Bonan *et al.*, 2014]. On longer timescales vegetation water use strategies regulate the global carbon and water cycles [De Kauwe *et al.*, 2015].

Many recent studies have aimed at advancing the representation of water flow through the Soil-Plant-Atmosphere continuum (SPAC) in land models [Xu *et al.*, 2016; Christoffersen *et al.*, 2016; Sperry *et al.*, 2017]. Explicit modeling of water flow through the SPAC adds complexity, but is consistent with evidence of dynamic regulation of vegetation water use in response to both soil and atmospheric drying [Sperry and Love, 2015]. Furthermore, via Darcy's Law, SPAC models have a robust physical basis. SPAC models involve new parameters, which presents new challenges [Drake *et al.*, 2017], but plant hydraulic trait information is available [Kattge *et al.*, 2011; Anderegg, 2015a], providing guidance on parameter estimation. and can be informative of forest vulnerability to drought [Choat *et al.*, 2012]. Likewise vegetation water status observations are available at a scale that is directly relevant to model development [Konings *et al.*, 2016; Grant *et al.*, 2016] and can be used to validate model results [Momen *et al.*, 2017; Konings *et al.*, 2017b].

The empirical representation of vegetation water stress in the Community Land Model (CLM) and other land surface models is a known deficiency, with implications for the representation of the dry/wet season in tropical rainforests [Powell *et al.*, 2013; Ukkola *et al.*, 2016].

In this study, we develop a plant hydraulic implementation within the recently released CLM version 5 (CLM5), based on hydraulic theory, which we refer to as the 'Plant Hydraulic Stress' (PHS) configuration. We analyse the dynamics of the new PHS model using site-level simulations that replicate the Caxiuanã, Brazil through-fall exclusion experiment [Fisher *et al.*, 2006].

Advancing the representation of the SPAC introduces the representation of vegetation water potential (discretized into leaf, stem and root elements) into the CLM, as well as an explicit representation of water supply, from the soil through the vegetation substrate. Tran-

64 spiration is attenuated with drought stress according to vegetation water status, capturing dy-
65 namic vegetation water use regulation. These changes have numerous implications, including

66 1. Leaf water potential serves as an improved metric for water status (compared to soil
67 water or soil matric potential), since it reflects vegetation sensitivity to both soil and atmo-
68 spheric drying, while serving as a diagnostic for excessive xylem tension and cavitation risk.

69 2. Modeling and plant hydrodynamics provides a framework for representing hydraulic
70 redistribution [Lee *et al.*, 2005]

71 3. Modeling vegetation water potential allows improved connection to remote sensing
72 observations (e.g. Vegetation Optical Depth) [Konings *et al.*, 2016].

73 4. Further, root water potential can be used to predict gradient-based root water uptake
74 based on Darcy's law, replacing the previous empirical transpiration partitioning heuristic.
75 This provides the means to vary, for example, the mean depth of extraction with changing
76 soil water conditions.

77 5. The new model can represent a range of water use strategies, improving the connec-
78 tion between plant carbon allocation decisions and water availability.

79 SAY IN WHICH SECTION WE WILL FINE EACH PART

80 To assess the new model formulation, we carried out site-level simulations at Caxiuanã
81 National Forest in Brazil, which features a critical biome (terra-firme moist tropical ever-
82 green forest). Starting in xxxx, a plot at this site was subjected to a x percent precipitation
83 through-fall exclusion. Due to the large drop in soil moisture at the precipitation exclusion
84 site, we expect and observe (Fisher *et al.* 2007) significant vegetation regulation of transpira-
85 tion and photosynthesis.

86 In this paper we 1. Introduce the PHS theory and implementation in the CLM 2. Ana-
87 lyze the dynamics of modeled water stress, root water uptake and soil moisture profiles. 3.
88 Compare PHS to the behaviour of the default CLM water stress configuration. 4. Discuss the
89 benefits and limitations of the new model.

90 2 Model Description

91 2.1 Photosynthesis

92 The CLM5 photosynthesis model is described in Bonan *et al.* [2011], Thornton and
93 Zimmermann [2007], and Oleson *et al.* [2013]. Photosynthesis is defined in three regimes:
94 Rubisco-limited, light-limited, and export-limited following Farquhar *et al.* [1980] and Harley
95 *et al.* [1992]. The implementation extends Sellers *et al.* [1996a,b] with co-limitation following
96 Collatz *et al.* [1991].

97 CLM5 photosynthesis, in its default configuration, is a two-big-leaf model, with a sun-
98 lit and shaded leaf for each plant functional type [Thornton and Zimmermann, 2007; Dai
99 *et al.*, 2004; Oleson *et al.*, 2013]. The canopy fluxes module iterates the solution for leaf tem-
100 perature to satisfy the leaf surface energy balance, while environmental conditions are evolv-
101 ing. Within this, the photosynthesis module further iterates to solve for inter-cellular CO₂
102 concentration, balancing stomatal flux of CO₂ with photosynthetic assimilation flux of CO₂.

103 2.2 Stomatal Conductance

104 CLM5 implements the Medlyn stomatal conductance model, which reconciles the em-
105 pirical and optimal approaches to modeling stomatal conductance [Medlyn *et al.*, 2011].
106 Stomatal conductance of CO₂ is thus directly related to net photosynthesis (A_n), CO₂ con-
107 centration at the leaf surface (C_a), and the square root of the vapor pressure deficit near the

leaf surface (\sqrt{D}).

$$g_s = g_0 + \left(1 + \frac{g_1}{\sqrt{D}}\right) \frac{A}{C_a} \quad (1)$$

The model features two parameters g_0 ($\mu\text{mol} / \text{m}^2 / \text{s}$) and g_1 ($\text{kPa}^{0.5}$). The g_0 parameter is minimum stomatal conductance, representing cuticular and epidermal losses (small). The g_1 parameter relates to the marginal water cost guiding the optimization of carbon assimilation. These parameters are plant functional type dependent.

The Medlyn model, derived from stomatal optimization theory, predicts stomatal conductance to maximize assimilation relative to water costs ($A - \lambda E$), but does not resolve concurrent limitations to stomatal conductance associated with drought conditions. These water stress factors (in our case, f_w), are used to represent stomatal and non-stomatal limitation not captured by the leaf-level stomatal conductance model (which can be thought of as a prediction of maximum stomatal conductance in these cases). To represent soil drought, and its impact on diffusive fluxes, land surface models typically include a ‘water stress factor’ (f_w , dimensionless, 0 to 1, formerly β_t). Uncertainty remains within the literature for how to apply water stress factors to photosynthesis and/or stomatal conductance. [Zhou *et al.*, 2013; Novick *et al.*, 2016b; Sperry and Love, 2015].

In CLM, f_w multiplies the rate of maximum carboxylation (V_{cmax}) as described in Oleson *et al.* [2013]. Other models opt for soil-moisture based stomatal limitation (linking the stomatal conductance model slope parameter to soil moisture), however, Lin *et al.* [2018] found that only g_0 was sensitive to soil moisture (and not g_1). Zhou *et al.* [2013] suggest that changes in assimilation tend to exceed those predicted by modulating g_1 with soil moisture, but could be captured by changing V_{cmax} . Other field studies, however, suggest that V_{cmax} does not change with drought, whereby modeled V_{cmax} instead may implicitly account for mesophyll conductance changes [Flexas *et al.*, 2004].

In PHS, we opt for a simplified form of this stress approach, which seems to be consistent with field observations [Lin *et al.*, 2018]. Prognostic water stress (f_w , ranging from 0-1) attenuates stomatal conductance indirectly via multiplication of V_{cmax} . Water stress then lowers assimilation, which is coupled to stomatal conductance ([Medlyn *et al.*, 2011]).

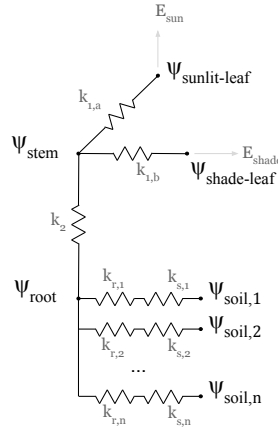
f_w is modeled here as a function of leaf water potential (ψ_{leaf}) (see Section 2.3.3), with stress increasing as ψ_{leaf} becomes more negative. This reflects the concept of hydraulic safety, with vegetation avoiding excessive xylem tension associated with risk of cavitation.

Utilizing leaf water potential adopts a framework where stomatal conductance optimized for carbon gain is concurrently limited by hydraulic constraints [Novick *et al.*, 2016b]. As a result, low soil water (bottom-up stress) can induce leaf moisture stress due to limited water supply while high atmospheric VPD can also induce leaf moisture stress by propagating a drying into the xylem (top-down stress).

Much recent work has focused on alternative constraints on plant hydrodynamics, especially in response to drying soils [Manzoni *et al.*, 2013a; Novick *et al.*, 2016b; Zhou *et al.*, 2014]. This includes how plants manage the risk of cavitation associated with increasing xylem tension [Sperry *et al.*, 1998]. [Sperry *et al.*, 2017], for example, argue that theory based on hydraulic costs (define) could be used instead of optimizing of $A - \lambda E$. Otherwise, the marginal water cost might be adjusted based on soil water status by adjusting λ or Medlyn g_1 [Manzoni *et al.*, 2013a], but this may underestimate drought effects on photosynthesis *expand on this-RF*[Zhou *et al.*, 2013; Lin *et al.*, 2018]. A hybrid approach, combines stomatal optimization with hydraulic constraints and/or so-called non-stomatal limitation, where stress attenuates V_{cmax} or mesophyll conductance (both of which feed back through photosynthesis to lower stomatal conductance) [Egea *et al.*, 2011; Novick *et al.*, 2016b]. [*link this back to which options are used in PHS -RF*]

155 2.3 Plant Hydraulic Stress (PHS)

156 The PHS model within CLM5 uses hydraulic (Darcy's) law and a corresponding elec-
 157 trical circuit analogy (Figure 1), to model the flow of water through the SPAC. The hydraulic
 158 framework is used to diagnose water stress associated with increasing xylem tension and to
 159 calculate the root water uptake in each of (in this case) 20 vertically discretized soil layers.



160 **Figure 1.** Plant hydraulic circuit analog schematic

161 2.3.1 Hydraulic schematic and segmentation

162 PHS solves for the set of SPAC vegetation water potential values (ψ_{root} , ψ_{stem} , $\psi_{\text{shade-leaf}}$,
 163 $\psi_{\text{sun-leaf}}$) that matches water supply (root water uptake) to water demand (transpiration),
 164 while maintaining continuity of water flow throughout the SPAC. Segmentation and other
 165 model design decisions followed a preference for a simplified implementation that whenever
 166 possible conformed to existing CLM model structure.

167 At each node in the circuit diagram in Figure 1 we model water potential, and, between
 168 nodes, we resolve the flux of water. The choice of nodes for segmentation is designed to take
 169 advantage of field-measured hydraulic traits and to allow for differences in segment parame-
 170 terizations [Simonin *et al.*, 2015; Sperry and Love, 2015]. As in other versions of the CLM,
 171 PHS uses vertically discretized soil layers and a two-layer (sunlit vs. shaded) canopy. Water
 172 uptake from the different soil layers is assumed to operate in parallel; a typical assumption
 173 justified by higher resistance in lateral versus central roots (e.g. Williams *et al.* 2001). We
 174 further separate resistance through the soil matrix from the resistance through the root tissue
 175 [Williams *et al.*, 1996]. Specifics on the parameterization of conductance for each segment
 176 are provided in Appendix B.1.

177 2.3.2 Water supply

178 Water supply is modeled via Darcy's Law, where flow of water (q) is the product of the
 179 path hydraulic conductance (k) and the gradient in water potential (accounting for changes in
 180 gravitational potential). Equation 2 represents the flow from a generic node 1 to node 2.

$$181 q = -k (\psi_2 - \psi_1 - \rho g \Delta z) \quad (2)$$

182 PHS does not represent plant tissue water storage (or capacitance, using the electrical
 183 circuit analogy). Capacitance significantly complicates the water potential solution [Celia
 184 *et al.*, 1990] and is challenging to parameterize [Bartlett *et al.*, 2016]. However, buffering

of water stress provided by tissue water storage could potentially be important especially on sub-daily timescales [Meinzer *et al.*, 2009; Epila *et al.*, 2017], whereby its inclusion may be warranted in future model generations.

Vegetation segment conductance is modeled following empirical xylem vulnerability curves [Tyree and Sperry, 1989], where segments lose conductance with increasing xylem tension related to cavitation and embolism [Holbrook *et al.*, 2001]. The vulnerability curves model loss of conductance relative to maximum conductance using two parameters: c_k , a sigmoidal shape-fitting parameter, and p_{50} , the water potential at 50% loss of segment conductance (following Gentine *et al.* [2016]).

Both c_k and p_{50} can be estimated from field experiments [Sack *et al.*, 2002], and p_{50} is available in the TRY trait database [Kattge *et al.*, 2011]. Parameterization based on p_{50} aligns with the call for a transition to models that use a wider range of plant functional trait data in their parameterization [Anderegg, 2015a]. The loss of xylem conductivity is based on lower terminal water potential (ψ_1) as is typical in other simplified models [Xu *et al.*, 2016], but may underestimate the integrated loss of conductivity [Sperry and Love, 2015].

$$k = k_{\max} 2^{-\left(\frac{\psi_1}{p_{50}}\right)^{c_k}} \quad (3)$$

PHS models root, stem, and leaf tissue conductances according to equation 3. The parameterization of k_{\max} varies by hydraulic segment (see details in Appendix B1). The conductance across the soil matrix to the root surface follows Williams *et al.* [2001] and Bonan *et al.* [2014] and estimates a characteristic distance between the bulk soil and the root surface, to facilitate length-scaling of soil conductivity. Bulk soil resistivity is based on Clapp and Hornberger [1978] as described in Oleson *et al.* [2013]. Further details are provided in Appendix B1.

2.3.3 Water demand

Vegetation water demand and stomatal regulation is based on the Medlyn stomatal conductance model (see Section 2.2), which we adjust using the water stress factor f_w . As discussed earlier, f_w is based on leaf water potential [Klein and Niu, 2014], and multiplies V_{cmax} , thus attenuating photosynthesis, and thus also stomatal conductance and transpiration.

As leaf water potential declines (because of transpiration) and xylem tension increases, transpiration is attenuated relative to its maximal value. The maximum transpiration ($E_{\text{sun,max}}$, $E_{\text{shade,max}}$) is defined as the value that results from Medlyn stomatal conductance in the absence of water stress (achieved by setting $f_w = 1$). The fraction of maximum transpiration is modeled with a two-parameter sigmoidal function (Equation 4).

$$\begin{aligned} E_{\text{sun}} &= E_{\text{sun,max}} 2^{-\left(\frac{\psi_{\text{sun-leaf}}}{\psi_{50}}\right)^{c_k}} \\ E_{\text{shade}} &= E_{\text{shade,max}} 2^{-\left(\frac{\psi_{\text{shade-leaf}}}{\psi_{50}}\right)^{c_k}} \end{aligned} \quad (4)$$

Where ψ_{50} is the leaf water potential at 50% loss of transpiration and c_k is a sigmoidal shape-fitting parameter.

We define f_w as the ratio of attenuated to maximal stomatal conductance (Equation 5). Maximum stomatal conductance ($g_{s,\text{sun,max}}$, $g_{s,\text{shade,max}}$) is computed as the stomatal conductance in the absence of water stress, i.e. $f_w = 1$. The attenuated stomatal conductance ($g_{s,\text{sun}}$, $g_{s,\text{shade}}$) is then the stomatal conductance associated with the PHS module water flow solution, which matches vegetation water supply with vegetation water demand (Section 2.3.4).

$$\begin{aligned} f_{w,sun} &= \frac{g_{s,sun}}{g_{s,sun,max}} \\ f_{w,shade} &= \frac{g_{s,shade}}{g_{s,shade,max}} \end{aligned} \quad (5)$$

Whereas the water supply parameters (see Section 2.3.2) relate to hydraulic traits often measured in the field, the hydraulic demand parameters ψ_{50} and c_k reflect the emergent property of hydraulic limitations to transpiration and must be empirically derived (WHAT ABOUT PLC CURVES?).

CLM also features two empirical stomatal control parameters, which are the soil matric potentials where stomata are either fully closed (θ_{wilt}) or fully open (θ_{crit}) (see Section 3). Recent modeling studies have proposed different forms of relationship between stomatal regulation with water stress [Sperry et al., 2017; Xu et al., 2016; Christoffersen et al., 2016] and thus this representation remains the topic of active research .

2.3.4 PHS solution

PHS solves for the set of vegetation water potential values (ψ) that matches water supply (root water uptake) to water demand (transpiration), while satisfying continuity across the four water flow segments (soil-to-root, root-to-stem, stem-to-leaf, and leaves-to-transpiration). At each time step, PHS computes the flux divergence f (representing the mismatch of flow in and out of each segment for a given set of vegetation water potential values ψ_i , and iteratively updates ψ until convergence is reached in terms of divergence, $f \rightarrow 0$.

$$\psi = \begin{bmatrix} \psi_{sun} \\ \psi_{shade} \\ \psi_{stem} \\ \psi_{root} \end{bmatrix} \quad (6)$$

$$f(\psi) = \begin{bmatrix} E_{sun} - q_{sun} \\ E_{shade} - q_{shade} \\ q_{sun} + q_{shade} - q_{stem} \\ q_{stem} - \sum_{j=1}^n q_{root,j} \end{bmatrix} \quad (7)$$

$$A = \frac{df}{d\psi} \quad (8)$$

While $|f| > 0$

$$\begin{aligned} \Delta\psi &= A^{-1}f(\psi_i) \\ \psi_{i+1} &= \psi_i + \Delta\psi \end{aligned} \quad (9)$$

The numerics are tractable because f has analytical derivatives and A (a 4x4 matrix with six null entries) is easy to invert when well-conditioned. Supply and demand converge, because transpiration demand decreases with more negative leaf water potentials and supply increases with more negative leaf water potentials. Within a set of PHS iterations (9), transpiration is assumed to be linear with f_w .

The PHS loop is nested within iterations for intercellular CO₂ concentration and leaf temperature. The non-linear relationship between f_w and transpiration is resolved through iteration for converging f_w alongside intercellular CO₂. Details on the numerical implementation are provided in Appendix Section B.1.

257 **3 Water stress factor, SMS vs. PHS**

258 PHS alters the transpiration beta function (β_t , colloquially BTRAN ,Equation 10),
 259 SAY WAHT IT IS which is the phenomenological soil water stress function in used in prior
 260 versions of CLM, as described in *Oleson et al.* [2013]. Because the name β_t is associated
 261 with this specific plant hydrodynamics representation, we opt to rename the variable to the
 262 water stress factor f_w . Throughout this paper we refer to the original CLM plant hydrody-
 263 namics framework as SMS (soil moisture stress), as compared to the newer implementation
 264 described here, PHS (plant hydraulic stress). We adopt this terminology (in lieu of CLM4.5
 265 vs. CLM5), because SMS is still deployable with CLM5. In this section we present the SMS
 266 version of f_w and outline the differences as compared to PHS

267 With PHS, we interpret f_w as a drought safety mechanism, attenuating stomatal con-
 268 ductance to avoid excessive xylem tension associated with very negative leaf water potential.
 269 As such, f_w is parameterized as a function of prognostic leaf water potential. With SMS,
 270 f_w is calculated based on soil matric potential, as a root-fraction weighted average potential
 271 departure from an empirical soil layer wilting factor (Equation 10). Recent studies suggest
 272 that the SMS parameterization introduces model bias in turbulent fluxes [*Bonan et al.*, 2014]
 273 and contributes to unrealistic drought response of photosynthesis and stomatal conductance
 274 [*Powell et al.*, 2013].

275 In SMS, the variable f_w is unitless, ranging from 0 to 1, with 1 corresponding to no
 276 water stress, and 0 corresponding to fully water stressed. It is calculated based on a root-
 277 fraction weighted average of soil layer wilting factor (w_i), which is a bounded linear function
 278 of soil water potential (ψ_i) relative to PFT parameters defining the soil potential with stom-
 279 ates fully open (ψ_o) and fully closed (ψ_c), among the soil layers $i = 1, \dots, n$. Note that root
 280 fraction (r_i) sums to 1, by definition.

$$f_w = \sum_{i=1}^n r_i w_i \quad (10)$$

$$w_i = 0 \leq \frac{\psi_i - \psi_c}{\psi_o - \psi_c} \leq 1 \quad (11)$$

283 **3.1 Root water uptake in SMS vs. PHS**

284 Such parameterizations (WHICH ONES?) have primarily been examined with appli-
 285 cation to stomatal conductance, but they are also used to define vegetation soil water extrac-
 286 tion. Each timestep, the transpiration flux solution must be distributed among the vertically
 287 discretized soil layers. In the SMS framework, the transpiration sink is partitioned by layer
 288 according to the soil layer wilting factor and root fraction.

289 In both stress parameterizations, f_w multiplies V_{cmax} to attenuate photosynthesis and
 290 stomatal conductance with soil water stress. With SMS, it is also directly used for modeling
 291 vegetation water extraction from the soil column. The total transpiration (T) is partitioned
 292 among the soil layers based on the f_w wilting factor. Within each soil layer, the contribution
 293 to total transpiration (q_i) depends on the layer root fraction and wilting factor, normalized by
 294 f_w :

$$q_i = \frac{r_i w_i}{f_w} T \quad (12)$$

296 Contrary to the heuristic SMS parameterization, the PHS implementation adopts a
 297 physically-based hydraulic framework, where the root water uptake (q_i) is the product of the
 298 hydraulic conductance (k_i) and the gradient in water potential ($-\Delta\psi$) driving the flow, i.e.
 299 obeying Darcy's law. That gradient is the difference between the root water potential (ψ_{root})

300 and the layer soil water potential (ψ_i), minus changes in gravitational potential, following
 301 Darcy's law.

$$\begin{aligned} q_i &= -k_i \Delta\psi \\ \Delta\psi &= (\psi_{\text{root}} - \psi_i - \rho g \Delta z) \end{aligned} \quad (13)$$

303 For comparison between SMS and PHS, we recast (12) into the hydraulic framework:
 304 defining T_{\max} , such that: $T = f_w T_{\max}$ to replace T in (12), and replacing w_t in (12) with the
 305 formula from (11).

$$q_i = \frac{T_{\max}}{\psi_o - \psi_c} r_i (\psi_i - \psi_c) \quad (14)$$

307 This yields SMS analogs for the hydraulic conductance and gradient terms of Equation
 308 13.

$$\begin{aligned} k_i &= r_i \frac{T_{\max}}{\psi_o - \psi_c} \\ \Delta\psi &= \psi_c - \psi_i \\ \text{constrained by: } \Delta\psi &= \begin{cases} 0 & \text{if } \psi_i < \psi_c \\ \psi_c - \psi_o & \text{if } \psi_i > \psi_o \end{cases} \end{aligned} \quad (15)$$

310 We use this formulation to discuss some of the implications for root water uptake from
 311 the former SMS parameterization of water stress (Equation 15).

312 3.2 Constant pulling potential

313 With SMS, that gradient is defined for each soil layer as the difference between the
 314 soil water potential in that layer (ψ_i) and a constant parameter, the soil water potential when
 315 stomata are fully closed (ψ_c). This parameter serves as the vegetation "pulling" potential for
 316 calculating the soil transpiration sink.

317 Using a constant wilting point is inconsistent with extensive evidence from the field of
 318 dynamic vegetation water potential, and cohesion tension theory (CITATIONS NEEDED)
 319 driving the transpiration flow. Likewise the values for ψ_c are quite negative, (-2.5 MPa for
 320 broadleaf evergreen tropical, BET, forests). *Fisher et al.* [2006] measured midday stem po-
 321 tential consistently higher than -0.5 MPa during the wet season, and on average -1.69 and
 322 -1.53 MPa during the dry season in the control and exclusion plots, respectively.

323 3.3 Conductance dynamics

324 In SMS, in lieu of dynamic vegetation water potential, intra-day SMS soil sink dynamics
 325 derive from a highly variable conductance (CLARIFY). As inferred in Equation 15, SMS
 326 conductance is modeled as a function of T_{\max} , and three constant parameters. T_{\max} is highly
 327 dynamic, responding to the diurnal course in transpiration demand. This is inconsistent with
 328 general principles of porous media flow, where conductivity is a function of the hydraulic
 329 architecture and its wetted status. Likewise, this representation of conductance does not rep-
 330 resent the characteristic phenomenon where vessels lose conductance with drying.

331 3.4 No dependence on belowground carbon allocation

332 As is typical in water stress parameterizations, the SMS conductance is scaled by layer
 333 using an area basis, here using the relative vertical root fraction is used. With PHS, an abso-
 334 lute measure of root biomass is used (see Appendix Equation B.7), so that the belowground
 335 water cycle interacts with carbon allocation to the roots. An absolute measure better con-
 336 forms with the physics of porous media flow and better responds to varying carbon allocation

337 strategies. For example, with SMS, if root mass doubles in every soil layer, the root access to
 338 water remains unchanged.

339 **3.5 Lacks penalties for extraction from depth**

340 Both PHS and SMS account for the effect of decreasing root area with depth (PHS,
 341 root area; SMS, root fraction), but PHS implements two other penalties for extracting water
 342 from deep in the soil column that are missing from SMS. The first is minor, but water ex-
 343 tracted from depth must overcome gravity, amounting to about 0.01 MPa per meter in depth.
 344 This is missing from SMS and included with PHS. Likewise, SMS ignores the fact that hy-
 345draulic conductance is generally taken to scale with the inverse of conducting length. Deeper
 346 roots feature longer root tissue conducting length, and root spacing within the soil is less
 347 dense, requiring longer conducting distances across the soil matrix. In PHS, both these pro-
 348 cesses result in diminished hydraulic conductance (UNCLEAR).

349 **3.6 Constraints**

350 With SMS, the gradient in water potential is constrained between 0 and the range of
 351 soil potential between parameters for stomata fully open and closed (Equation 15). The up-
 352 per constraint caps the gradient in water potential when soil potential reaches the value for
 353 stomata fully open ($\psi_o = -0.65$ MPa for BET). Darcy's Law predicts that the gradient in water
 354 potential would continue to increase until saturation matric potential. The lower constraint
 355 caps the gradient in water potential at zero, disallowing negative gradients. However, re-
 356 versed water fluxes, caused by positive gradients in water potential from root to soil, have
 357 been observed in the field [Burgess *et al.*, 1998]. Both constraints are eschewed with PHS.

358 **4 Experiment Description**

359 All four simulations in this paper use the same development version of CLM5 (devel-
 360 opment version r270, https://github.com/ESCOMP/ctsm/releases/tag/clm4_5_18_r270).

361 The four simulations are used to assess the impact of the plant hydrodynamics model
 362 (PHS vs. SMS) on a through-fall experiment (i.e., with either ambient or 60% through-fall
 363 excluded), with all other model components and forcing shared. Simulations are run offline
 364 (uncoupled from an active atmospheric model), spanning from 2001 through 2003, utilizing
 365 the satellite phenology (SP) mode of CLM5 in which vegetation state (LAI, canopy height) is
 366 prescribed and biogeochemistry is inactive. All simulations start from the same initial con-
 367 ditions, which are obtained from a 9-year spin-up that repeats the PHS/Ambient simulation
 368 three times. To avoid duplication, descriptions of site characteristics, forcing data, and obser-
 369 vational sap flux, can be found in Fisher *et al.* [2007].

370 **4.1 Parameter Values and Through-fall Exclusion**

372 Selected parameter values concerning vegetation hydrodynamics are presented in Table
 373 1. All other parameters use the default values associated with the r270 version of CLM5. In-
 374 formed by Fisher *et al.* [2008], we tuned soil hydraulic parameters and through-fall exclusion
 375 rates to reasonably capture the observed soil water dynamics (Fisher *et al.* [2007] Figure 4),
 376 Supplementary Figure A.1. Likewise, we tuned k_{max} and g_1 parameters to improve the fit
 377 to sap flux observations in the ambient simulation. The object of this paper is to present the
 378 dynamical impact of PHS to clearly describe model functionality. Model skill and parameter
 379 sensitivity will be assessed in follow-up studies.

371

Table 1. Select parameter values

CLM name	Full Name	Symbol	Value
kmax(1)	Maximum Sun Branch Conductance	$k_{1a,\text{max}}$	4e-7 s ⁻¹
kmax(2)	Maximum Shade Branch Conductance	$k_{1b,\text{max}}$	4e-7 s ⁻¹
kmax(3)	Maximum Stem Conductivity	$k_{2,\text{max}}$	4e-7 m/s
krmax	Maximum Root Conductivity	$k_{r,\text{max}}$	6.3e-9 m/s
psi50	Water potential at 50% loss of conductivity	ψ_{50}	-2.45 MPa
ck	Vulnerability shape parameter	c_k	3.95
smpso	Soil potential with stomata fully open	ψ_o	-0.647 MPa
smpsc	Soil potential with stomata fully closed	ψ_c	-2.5 MPa
medlyn_intercept	Medlyn intercept	g_0	100 $\mu\text{mol} / \text{m}^2 / \text{s}$
medlyn_slope	Medlyn slope	g_1	7 kPa ^{0.5}
n	Soil porosity	n	0.42
hksat	Saturated soil hydraulic conductivity	$k_{s,\text{max}}$	1.5e-5 m/s
sucsat	Saturated soil matric potential	ψ_{sat}	461 Pa
bsw	Brooks-Corey parameter	b	6

^aTable note text here.

380

5 Analysis Details

381

5.1 Water potential

382
383
384
385

Annual and diurnal cycles of vegetation water potential are presented. For the diurnal cycle, we average by timestep over the 91 days of SON, 2003, reporting curves for root, stem, shade-leaf, and sun-leaf water potential. For the annual cycle, we plot monthly mean midday (local time 12:00 to 14:00) sun-leaf water potential.

386

5.2 Stress factor, annual cycle

387
388
389
390
391

Monthly means are reported for transpiration, gross photosynthesis, and f_w , the water stress factor (Fig 3). For the water stress factor, we opt to report the midday water stress averaging over local time 12:00 to 14:00. Monthly mean observational sap flow is also shown, courtesy of Fisher *et al.* [2007], which reports details on scaling observations to stand level. Months were dropped that featured fewer than 5 days of data.

392

5.3 Stress factor, diurnal cycle

394
395
396
397
398
399
400
401
402
403

In Figure 4, we plot the diurnal cycle of the stress factor averaged over the 2003 dry season (SON) (I am not a big fan of sentences in Figure we show, better to say what ahppens and then refer to figure). Drivers of the stress function are examined in Figure 5. To highlight the response of stress to VPD, we subsetted data according to downwelling solar radiation, which also influences stress. Data are selected with downwelling solar radiation between 400 and 425 W/m², which corresponds to 775 half-hour timesteps. For the TFE simulations, (Figure 5c,d), we additionally exclude data from 2001, because TFE was not initiated until November 2001, leaving 515 timesteps. Data are subdivided into terciles based on soil water (within each plot), and colored accordingly. The terciles are defined for each simulation in Table 2.

404

5.4 Hydraulic conductance

405
406

In Figures 6 and 7, we compare conductance values derived from the PHS and SMS implementations. With SMS, k is not explicitly modeled, so instead we infer k , by dividing

393

Table 2. Root-zone soil potential terciles for Figure 5

Simulation	T1	T2
PHS, Ambient	-0.0136 MPa	-0.0476 MPa
PHS, TFE	-0.0788 MPa	-0.2454 MPa
SMS, Ambient	-0.0056 MPa	-0.2296 MPa
SMS, TFE	-0.6474 MPa	-1.8467 MPa

407
408
409
410
411

root water uptake q_i , by $\Delta\psi$ as defined in Equation 15. We interpret the constraint that $\Delta\psi$ be greater than or equal to zero to mean that conductance is zero in non-conforming cases, which we extend to $k = 0$ when $\Delta\psi < 1$ kPa. For our analyses, we consider only points when transpiration is greater than 4 W/m², which improves the tractability of inferring conductance, given that SMS root water uptake is precluded absent transpiration (REPHRASE).

412
413
414
415
416

For Figure 6a,b, conductance is plotted from Soil Layer 3 (spans from 6 to 12 cm below ground), for all points during 2003 when transpiration is greater than 4 W/m² (n=7752). For Figure 7a,b, conductance is averaged daily, subject to the same restrictions. Average intra-day standard deviation is reported for FMA, by which we calculate a daily standard deviation of complying points, and report the average over the 89 days.

417

5.5 Root water uptake

418
419
420
421
422
423
424
425
426
427

Vertical profiles of the rate of root water uptake are presented in Figures 8a and 9a, averaged over SON and FMA, respectively. This is plotted as average cumulative rate of root water uptake, starting at depth (8.6 meters). Time series of total root water uptake are also provided (Figs 8b,c, 9b,c). We plot total cumulative water extracted from near the surface over time in Figures 8b and 9b, accompanied by that extracted from depths beyond 20 centimeters in Figures 8c and 9d. We chose 20 centimeters as the break point based on the vertical profiles of root water uptake, and with a preference for not splitting any of the discrete soil layers. Soil Layers 1-4 span 0 to 0.2 meters, and Soil Layers 5-20 span 0.2 to 8.6 meters. Time series of total cumulative ambient precipitation are shown for comparison (Figs 8b and 9b).

428

5.6 Hydraulic redistribution

429
430
431
432
433
434
435
436
437
438

Hydraulic redistribution refers to flows of water between soil layers through vegetation substrate. To calculate total HR, we sum the negative root water uptake fluxes ((i.e., root to soil fluxes) across all soil layers. Total HR, partitioned by month and by daytime versus nighttime is shown in Figure 10. Note that over the course of a day or season, HR can occur without net negative root water uptake. For example, hydraulic lift may occur at night, moving water from deep in the soil column up to near the surface, which is then more readily available for transpiration during the following day. This can result in HR occurring even when there is net positive root water uptake. This type of feature is evident in Figure 8, where there is net positive root water uptake throughout the soil column over the 2003 dry season, even when there is significant HR into the near-surface layers (Fig 10).

439

5.7 Soil moisture

440
441
442
443
444

The vertical profile soil water potential under 60% TFE is plotted in Figure 11 (SMA, DO NOT SAY THIS IS PLOTTED BUT DESCIRBE RESULTS AND MENTION FIGURE). The range in soil potential is much larger within the SMS paradigm, which made it difficult to plot both panels with the same color scale. In order to preserve information in

444 the PHS plot, we opt for a scale of 0 to -1 MPa, as compared to 0 to -3 MPa for SMS. When
 445 comparing column average soil potential, we use separate definitions, which reflect each
 446 paradigm's representation of soil water availability. With SMS, we opt for a root-fraction
 447 weighted average, following from Equation 14. This is a poor measure for PHS, because it
 448 neglects gravitational contributions and the appropriate root area basis. Instead we opt for
 449 predawn (defined at 5AM) root water potential, which, given minimal transpiration at night,
 450 is in equilibrium with the soil column.

451 **6 Results and Discussion**

452 **6.1 Modeling vegetation water potential**

453 The models are compared for the 2003 dry season (Sept-Oct-Nov or SON) at Caxiuana
 454 for two experiments: the first with ambient rainfall (AMB), and the second with 60% of rain-
 455 fall excluded, or 'through-fall exclusion' (TFE), Figure 2.

456 In the ambient simulation (Fig 2a), average midday water potentials are -1.96, -1.95,
 457 -1.94 MPa for sunlit leaf, shaded leaf, and stem, respectively. With through-fall exclusion
 458 (TFE), as expected the midday water potentials decrease to -2.77, -2.76, -2.75 MPa, respec-
 459 tively (Fig 2b).

460 Both panels show the characteristic drop in water potential around midday and the ex-
 461 pected sequencing with the leaf water potentials more negative than the stem potential, which
 462 is more negative than the root potential. The sequencing is difficult to distinguish from the
 463 plot, where the stem, sunlit, and shaded leaf water potential curves nearly overlap for both
 464 experiments because there is only very small drop in potential between the stem and leaves.

465 The small difference between leaf and stem water potentials results from minimal re-
 466 sistance to water flow across these segments. (LINK THIS TO THE PREVIOUS STATE-
 467 MENT) The current PHS parameterization of stem-to-leaf resistance is relatively simple
 468 compared to the literature [Franks *et al.*, 2007] and could be advanced in future versions.

469 TFE lowers average midday sunlit leaf water potential by 0.81 MPa compared to the
 470 ambient simulation, during SON-2003 (dry season). This change in leaf water potential can
 471 be partitioned into the change in soil water potential, the change in potential drop from soil-
 472 to-root, and the change in potential drop from root-to-leaf.

473 Beginning with the change in soil water potential, in the ambient simulation, average
 474 predawn (5AM) root water potential (an integrated measure of soil water potential) is -0.075
 475 MPa. With TFE, it falls to -0.36 MPa, resulting in a decrease in predawn root water potential
 476 of 0.28 MPa relative to the ambient simulation. The difference between midday and predawn
 477 root water potential (which stands in for potential drop from soil-to-root) is lowered by 1.06
 478 MPa in the simulate TFE plot (from -0.06 MPa, ambient, to -1.12 MPa, TFE).

479 The difference between sunlit leaf and stem water potential at midday acts in the oppo-
 480 site direction, changing from -1.83 MPa in the ambient simulation to -1.29 MPa with TFE,
 481 attenuating the drop in leaf water potential by 0.54 MPa.

482 Predicted water potential values are comparable with field observations, where average
 483 dry season leaf water potential was measured as -2.47 MPa [Fisher *et al.*, 2006]. With PHS,
 484 modeled change in leaf water potential due to TFE is -0.81MPa, which can be partitioned
 485 into -0.28 MPa predawn root water potential, -1.06 soil-to-root drop, +0.53 root-to-leaf drop.
 486 The drop in water potential across the stem partially abates the change in the soil and roots
 487 due to TFE.

488 Though stem conductance decreases with drying, transpiration also decreases, yield-
 489 ing a net effect of a smaller drop in water potential across the stem. This is consistent with
 490 findings in Fisher *et al.* [2006] that most of the whole-plant resistance is above ground, but

491 that added resistance from drying is predominately sourced? below ground. Likewise *Fisher*
 492 *et al.* [2006] found evidence of isohydric behavior, where plants manage water loss through
 493 stomata to regulate leaf water potential, which is consistent with results here of reduction in
 494 potential drop across the stem. However, PHS shows declines in midday leaf water potential
 495 due to TFE, but *Fisher et al.* [2006] found no significant observed difference between ambi-
 496 ent and TFE dry season leaf water potential. This could indicate that our parameters do not
 497 result in sufficiently isohydric behavior.

498 Many facets of our hydraulic representation are simplified relative to the literature, re-
 499 reflecting that in a model designed to operate at the global scale, there is a tradeoff between
 500 added complexity and parameter reduction. The current PHS parameterization omits vegeta-
 501 tion capacitance, which may be important for accurately modeling the diurnal cycle of water
 502 stress especially in tropical rainforests [*Meinzer et al.*, 2009]. Further, hydraulic conductance
 503 hysteresis and permanent cavitation are absent from the PHS vulnerability parameterization,
 504 whereby xylem segments fully regain conducting capacity upon re-wetting. This limits the
 505 influence of drought legacy, which has been shown to be significant for forest mortality [*An-*
 506 *deregg et al.*, 2013b].

507 Similar to other simplified models [*Xu et al.*, 2016], loss of conductance is based on
 508 lower terminus water potential, which may underestimate integrated loss of conductivity
 509 [*Sperry and Love*, 2015]. These simplifications each serve to lessen the parameter and/or
 510 computational burden of PHS. Our objective was to simplify the plant hydraulic representa-
 511 tion for this initial implementation, acknowledging that more comprehensive process repre-
 512 sentation may prove necessary for future model versions.

513 6.2 Stress factor, annual dynamics

514 Figure 3 shows monthly mean values of the water stress factor, gross primary produc-
 515 tivity, and transpiration over the three-year simulations for PHS versus SMS under ambient
 516 and 60% through-fall exclusion conditions. Under ambient through-fall conditions, the SMS
 517 simulation features less stress (Fig 3b), with no stress ($f_w > 0.99$) in 24 out of 36 months.

518 PHS predicts more stress (Fig 3a), with stress in sync with the evolution of midday leaf
 519 water potential (Figure 2). As a result, f_w is generally lowest in September (Fig 3e). ZQZ
 520 need to go back and output btran proper. Alternatively, SMS predicts no stress ($f_w > 0.99$)
 521 during any of the three Septembers of the ambient simulation. Instead f_w is generally lowest
 522 in December.

523 SMS has the most stress in December, which is associated with lower soil moisture
 524 (Supp Fig ??). While soil moisture is lowest in December, transpiration demand is higher
 525 in September, which is the month with the most stress in the PHS simulations (Fig3a). To
 526 achieve high transpiration rates, vegetation must operate with a large gradient in water po-
 527 tential from soil-to-leaf, associated with increased xylem tension and risk of cavitation. As
 528 such, leaf water potential declines with soil moisture drying, but also with increasing tran-
 529 spiration demand (Fig 2). PHS is designed to represent hydraulic limitation to transpiration
 530 associated with xylem tension, which responds to both soil drying and increased transpira-
 531 tion demand (i.e. higher VPD) [*Sperry and Love*, 2015]. The latter is absent from the SMS
 532 formulation.

533 Through-fall exclusion (which initiates on November 1, 2001) adds stress in both the
 534 SMS and PHS simulations (Fig3c,d) . The added stress is greater and the onset faster with
 535 SMS. In both cases, the effect of TFE accumulates in time, with less photosynthesis and tran-
 536 spiration in 2003 compared to 2002. This is not reflected in the sap flux observations, which
 537 feature a more rapid onset of reduced transpiration, and similar transpiration between 2002
 538 and 2003.

539 In both SMS and PHS, soil water is used to buffer shortfalls in precipitation versus
 540 transpiration (Supp Fig A.9). (UNLCEAR). Transpiration in PHS is less sensitive to TFE,
 541 which can be partly attributable to differences in root water uptake (see Section 6.5). PHS
 542 utilizes more deep soil water to mitigate declines in root-zone soil moisture as water flow
 543 is imposed to go down water potential gradients. In the dry season surface drying also de-
 544 creases soil-root conductance so that it is easier to extract moisture from deeper layers, con-
 545 sistent with observations based on isotopes (CITATION).

546 Another dynamic feature of PHS is that hydraulic limitation establishes a negative
 547 feedback loop between photosynthesis/transpiration and water stress. If photosynthesis in-
 548 creases, generally stomatal conductance and transpiration increase. This causes more nega-
 549 tive leaf water potential and an associated increase in water stress, which attenuates photo-
 550 synthesis. This diminishes variability in transpiration and photosynthesis, relative to SMS
 551 (Fig 3c-f). The strength of this feedback is subject to parameters controlling maximum con-
 552 ductance and the stomatal response to leaf water potential. Quantifying variability in diffu-
 553 sive fluxes with PHS as compared to SMS and observations is an important topic for future
 554 studies (See Lawrence et al in prep).

555 Significant uncertainty exists in soil and root hydraulic parameters as well as the root
 556 distribution, whereby better behavior may exist within the plausible parameter space. Like-
 557 wise, the parameter values for both stress implementations could be tuned further. Observa-
 558 tions indicate the trees here adopt an isohydric behavior, where declines in soil moisture are
 559 tightly coupled with reduced transpiration, which mitigates decreases in leaf water potential
 560 [Fisher et al., 2006]. The parameter values employed for these simulations may be insuf-
 561 ficiently isohydric (GIVE REFERENCE AND DEFINE ISOHYDRICITY), which could
 562 explain limited sensitivity to TFE relative to observations.

563 6.3 Stress factor, diurnal dynamics

564 In addition to changes in the annual cycle, PHS introduces a diurnal cycle to f_w (Fig
 565 4a). The SMS version of f_w exhibits almost no diurnal variability (Fig 4b) since water stress
 566 is therein a function of soil water potential, which lacks a significant diurnal cycle. PHS uses
 567 a function of leaf water potential (e.g. Fig 2a,b) to model water stress, which responds to
 568 diurnal variation in transpiration demand (via changes in VPD, solar radiation, etc.).

569 The relationship of water stress with VPD and soil potential is shown in Figure 5. To
 570 emphasize the relationship with VPD, data are subsetted for a small window in downwelling
 571 solar radiation (between 400 and 425 W/m²). For the TFE simulations (panels c and d), we
 572 also subset for years 2002 and 2003, because TFE was not active during most of 2001. Points
 573 are colored based on soil potential, partitioning the data from each plot into terciles, blue
 574 points are wettest, red points driest, and yellow points intermediate. For details on the soil
 575 water classification and radiation subsetting see Section zqz (THIS SHOULD BE IN CAP-
 576 TION NOT MAIN TEXT).

577 The SMS version of f_w has a clear dependence on soil potential, but no relationship
 578 with VPD (Fig 5b,d), as expected. Drier soil potentials are associated with lower values
 579 of f_w (which corresponds to more stress). With PHS, higher VPD results in more stress
 580 (Fig5a,c). Under ambient through-fall conditions (Fig5a), soil water potential has minimal
 581 influence. With TFE, stress responds to both VPD and soil water (Figure 5c). Similar effects
 582 are shown in response to downwelling solar radiation (Supp Fig A.2).

583 Water stress is applied to capture limitations with declining water status that are not
 584 reflected within the Medlyn stomatal optimization theory (which only optimizes $\delta E/\delta A$,
 585 and thus does not take water supply into account). CLM implements non-stomatal limita-
 586 tion by multiplying V_{cmax} by f_w . Though there is limited evidence of down-regulation of
 587 V_{cmax} [Flexas et al., 2006], this was the best option within CLM for applying stress through
 588 the GPP term of the stomatal conductance model, in accordance with field observations [Lin

589 *et al.*, 2018; Zhou *et al.*, 2013]. If in future versions of CLM, mesophyll conductance is rep-
 590 resented, it may be a more appropriate avenue for achieving the same effect. (MERGE WITH
 591 PREVIOUS DISCUSSION, TRY AVOIDING REPETITIONS A MUCH AS POSSIBLE)

592 Total soil water content (or departure from saturation) is a typical basis for diagnos-
 593 ing water status and stress [Drake *et al.*, 2017], which is in line with an SMS-type approach.
 594 While capturing supply limitations, this framework neglects effects of transpiration demand
 595 on xylem tension. Given constant stomatal conductance, xylem tension increases with de-
 596 clining soil water, but also with increasing vapor pressure deficit. While VPD sensitivity is
 597 included in the Medlyn model, it serves to mitigate increasing water costs, without consider-
 598 ation of cavitation. Evidence suggests that vegetation employ water use strategies to mitigate
 599 the risk of cavitation associated with increasing xylem tension [Sperry *et al.*, 1998; Fisher
 600 *et al.*, 2006; Choat *et al.*, 2012]. Utilizing leaf water potential as the basis for water status
 601 reflects this constraint. This may be especially important given projected increases in VPD
 602 associated with warming.

603 **6.4 Hydraulic conductance: PHS vs SMS (implied)**

604 Soil-to-root conductance (k_{sr}) is explicitly represented in PHS, modeled as a function
 605 of soil potential (zqz). With SMS, k_{sr} is not explicitly modeled, but it can be inferred, by
 606 dividing root water uptake by the gradient in water potential (see Section zqz). Comparing
 607 conductance under these two paradigms serves to highlight differences in how water supply
 608 is modeled. In , we plot the time-series of conductance values from Soil Layer 3 (spanning
 609 from 6 to 12 centimeters below the surface) under ambient through-fall conditions during
 610 2003, along with precipitation over the same period (PLUG IN CAPTION).

611 During the wet season, PHS conductance is greater than SMS by more than two orders
 612 of magnitude (Fig 6a,b). PHS conductance is generally steady through the wet season (Fig
 613 6a), followed by a slow decline over the dry season with short resurgence episodes associ-
 614 ated with rain events. The SMS implied conductance features more variability relative to the
 615 mean (Fig 6b). During FMA-2003, average intra-day standard deviation of Layer 3 conduc-
 616 tance is $4.6e-12 \text{ s}^{-1}$ with PHS and $9.9e-12 \text{ s}^{-1}$ with SMS. In an absolute sense the SMS stan-
 617 dard deviation is about twice as large as PHS. The difference is larger in a relative sense, as
 618 this corresponds to 0.08% of the mean FMA conductance with PHS and 62.9% of the mean
 619 FMA conductance with SMS.

620 The SMS inferred conductance is tethered to transpiration (see Section 3), which leads
 621 to the high variance and a clear diurnal cycle (Supp Fig A.3). Instead PHS calculates k_{sr}
 622 based on soil hydraulic properties and root xylem vulnerability, which better reflects the
 623 physics (flow has to be down water potential gradients) and the temporal dynamics of tran-
 624 spiration demand.

625 As a result conductance is less variable, with the expected responses to drydown (loss
 626 of conductance) and re-wetting (increased conductance). This is further demonstrated in Fig-
 627 ure 7, where we plot the daily mean conductance from Soil Layer 3. With 60% through-fall
 628 exclusion (Fig7a, dotted line), PHS conductance decreases, whereas with SMS, the daily
 629 mean conductance increases (Fig7b). The latter SMS increase is unrealistic and conflicts
 630 with extensive literature demonstrating loss of conductivity with drying (CITATIONS).

631 Despite two orders of magnitude difference in conductances, total root water uptake
 632 during FMA2003 is not very different (23.4 cm PHS vs. 24.9 cm SMS). The reason for these
 633 smaller differences, is that the extraction gradient compensate for the differences in con-
 634 ductance. The SMS extraction gradient is measured relative to ψ_c (a parameter defining soil
 635 potential with stomates fully closed), which equals -2.5MPa for BET. The PHS extraction
 636 gradient is relative to root water potential which during 2003 (ambient through-fall) varies
 637 between -0.02 and -0.23 MPa. Fisher *et al.* [2006] measured stem water potential consis-
 638 tently higher (less negative) than -0.5MPa.

With TFE, PHS Layer 3 conductance can approach the values seen in SMS. The average Layer 3 conductance with PHS for August 2003 (60%TFE) is $4.75 \times 10^{-11} \text{ s}^{-1}$ as compared to $3.89 \times 10^{-11} \text{ s}^{-1}$ for SMS. This is a result of the orders of magnitude response of PHS soil-to-root conductance to changes in soil potential (Supp Fig A.4) (UNCLEAR MODIFY SENTENCE). This conforms with typical soil hydraulics, where large changes in conductance occur with drying. On the other hand, SMS conductance has no clear relationship with soil potential (Supp Fig A.4).

6.5 Root Water Uptake: PHS vs SMS

Root water uptake is the flux of water (q_i , mm/s) extracted from each of the vertically discretized soil layers ($i = [1, 2, \dots, n]$). These fluxes are used as the soil transpiration sink terms within the Richards' equation [Oleson *et al.*, 2013] and, summed over the soil column, are equivalent to the transpiration flux. As described above (and in Section 3), PHS adopts a hydraulic framework for root water uptake.

PHS simulations (black color), feature more surface extraction than with SMS, especially under ambient through-fall conditions (Fig8a), during the 2003 dry season. The time-series of PHS total cumulative extraction (cm) from near-surface soil (Fig8b) responds to precipitation (Fig8d), with increased surface extraction after rain events.

Under ambient conditions the SMS partitioning of extraction between near-surface and depth is not sensitive to precipitation. In PHS near-surface extraction decreases by 40% with TFE (8.12 vs 13.51 cm), while, SMS features a 24% increase in absolute terms (5.28 vs 6.55 cm, Fig 8b). Under TFE, both PHS and SMS extract minimal water from between 0.5 and 4m, (3.18 cm and 0.56 cm, respectively, over the three months). Both compensate by increasing extraction from below 4m, but PHS to a much larger extent, which corresponds to overall significantly more root water uptake during TFE.

Root water uptake dynamics respond to changes in hydraulic conductance and/or changes in the gradient in water potential. PHS has more access to water at depth under TFE, associated with higher conductance values. With decreasing soil potential, hydraulic conductance decreases with PHS, but can increase with SMS (6.4). Instead SMS is limited by the extraction gradient, with root water uptake declining to zero as soil potential approaches -2.5 MPa (Supp Fig A.5). PHS is more sensitive to changes in soil water potential, with stronger decreases in root water uptake in response to drying within a soil layer (Supp Fig A.5). In response, PHS features increases in near-surface water uptake after rain and decreases with TFE.

The wet season (Feb-Mar-Apr FMA-2003), features more and steadier rain (Fig 9d). PHS responds with an increase in the proportion of water extraction from near the surface relative to SON. Under ambient conditions net extraction is zero beyond about 38 centimeters depth (Fig 9a, solid black line). In comparison, SMS extracts more than half its water from beyond 1 meter in depth even during the wet season (Fig 9a, solid gray line). With TFE, PHS extraction is negative beyond 20 centimeters, indicating hydraulic redistribution (Fig 9c). Over the three month FMA-2003 period, there is no net root water uptake below 20 centimeters depth, but rather a deposition of about 10 cm of water is simulated.

In both the wet and dry season, PHS features significantly more root water uptake from the near-surface layers (0 to 20cm in depth). Modeled surface extraction is especially high over the wet season under through-fall exclusion conditions, summing to 32.7 cm over 89 days. By comparison SMS extracts 4.8 cm under the same conditions. With a soil porosity of 0.42, the top 20 cm of soil hold only 8.2cm of water at saturation.

Conductances are higher with PHS (see Section 6.4), which allows for higher rates of root water uptake, especially from moist soil layers. Likewise PHS better reflects penalties for extraction from depth (Section 3, favoring near-surface water all else being equal. The

688 highest rates of root water uptake (relative to layer size) occur from Soil Layer 2, after rain
 689 events during the dry season (Supp Fig A.7). Lowering maximum conductance can attenuate
 690 high rates of extraction, if observations conflict with model output.

691 The PHS configuration allows for more realistic root water uptake, incorporating hy-
 692 draulic theory. SMS does not accurately represent xylem loss of conductance or the dynam-
 693 ics of vegetation water potential. Both are difficult to parameterize, given the scarcity of data
 694 describing states, traits, and fluxes underground. PHS offers a process connection between
 695 soil potential and leaf water potential, which may be used to evaluate the model.

696 6.6 Hydraulic redistribution

697 During the wet season surface extraction supplies transpiration, but is also redistributed
 698 into lower soil layers. Hydraulic redistribution has been observed in the field [Oliveira *et al.*,
 699 2005], and is not represented in the SMS version of the CLM [Lee *et al.*, 2005]. which sets
 700 root water uptake to zero if the gradient in water potential is negative.

701 For HR to occur into a soil layer, the soil potential must be more negative (drier) than
 702 the ψ_{root} (see Figure . During the day, transpiration requires a gradient in water potential
 703 from soil-to-root, which lowers ψ_{root} , decreasing the amount of HR. Therefore, in PHS, more
 704 HR occurs at night, in accordance with observations and theory [Oliveira *et al.*, 2005; Lee
 705 *et al.*, 2005].

706 HR is predominately downwards during the wet season (FMA), serving to diminish the
 707 gradient between the newly-wetted surface and still-dry depths (Supp Figs A.6,A.7). Redis-
 708 tribution occurs in both directions during the dry season (SON), downwards after rain events,
 709 and upwards with drying. Only with TFE, and only during the dry season, is there significant
 710 extraction beyond 6 meters (Figs 8, 9). There is very little water deposited at depths beyond 6
 711 meters at any point in either simulation.

712 Under ambient conditions simulated HR in PHS totals to 41.3 cm (10.3 cm during the
 713 day, 31.0 cm at night), Figure 10. HR declines slightly to 37.0 cm (11.5 cm day and 25.5 cm
 714 night) with TFE. For reference, total transpiration over the same time period was 120 and 99
 715 cm for ambient and TFE conditions, respectively. The TFE simulation has less HR overall,
 716 but more HR during wet months, Feb-June.

717 Increased downwards? HR within the TFE plot occurs in Feb-June, associated with the
 718 drier TFE soils and larger gradients in soil potential from surface to depth. HR is lower in
 719 January, and July-December with TFE. Similar to during the wet months the gradient in soil
 720 potential (in this case from depth to surface) is larger with TFE. However, the soils overall
 721 are so dry with TFE during the dry months, that loss of conductance from soil-to-root coun-
 722 teracts the large gradient, resulting in lower HR.

723 The dynamics of HR with PHS align with observations, with more HR at night, and
 724 HR occurring in both directions vertically [Burgess *et al.*, 1998]. The absolute values of HR
 725 are difficult to assess, given limited observations.

726 In PHS, Allowing HR to occur into the top layer of the soil column significantly de-
 727 graded modeled soil evaporation (not shown). We opted to omit the first top Layer (span-
 728 ning 0 to 2 cm below ground) soil-to-root hydraulic conductance, to prevent HR from over-
 729 supplying water for soil evaporation.

730 6.6.1 Is hydraulic redistribution a feature or a liability?

731 HR is a natural consequence of using Darcy's Law to model root water uptake - when
 732 hydraulic gradients are reversed, HR should occur. As such it is naturally included within
 733 a plant hydraulics model with multiple soil layers and is an emergent behavior of respect-
 734 ing hydraulic flow down gradient of potentials. In ESMs, where soil moisture is typically

resolved vertically, interfacing the plant hydraulics with a multi-layer soil naturally accounts for HR. Other models, similar to the SMS paradigm, disallow HR by constraining root water uptake to be positive [Xu *et al.*, 2016].

Most literature models force the model with a single bulk soil water potential ψ_s , which precludes HR [Fisher *et al.*, 2007; Bonan *et al.*, 2014; Sperry *et al.*, 2017]. Christoffersen *et al.* [2016] expand beyond a single ψ_s horizontally, representing soil elements at different characteristic distances from the root surface, but still feature a single soil layer in the vertical dimension.

Likewise HR is likely sensitive to the representation of vegetation tissue capacitance and below-ground hydraulic segmentation (CITAIONS NEEDED).

Hydraulic redistribution has the impact of reducing the variance in the availability of water for plant transpiration, potentially at odds with observations of interannual variation (see Lawrence et al in prep. Tang et al. 2015) Observations of HR are extremely difficult, in unequivocal detection of HR involves the observation of reverse flow along transport roots, typically at rates close to the detection threshold of sap flow monitoring systems. Therefore, the degree to which HR actually occurs is unclear. While there is some first-order benefit to plants of moving water from deep soil to surface layers to allow more transpiration, this water is then also available for competition with other shallow-rooted plants, and for evaporative processes. Further, cavitation of fine roots in shallow soils might explicitly act as a 'fuse' to prevent loss of water from the plant into dry soil layers (Kotowska *et al.* 2015) - a process not explicitly resolved here. Therefore we view this first implementation of HR into the default versions of the CLM as a 'null' hypothesis for the functioning of this process, and as a platform to allow further refinement from the plant hydraulics community.

6.7 Soil moisture profile

The column total soil water in all four simulations is initialized at 2.66 meters (over an 8.6-meter soil column) (SAY WHY). The change in total soil water is small under ambient conditions, decreasing by 0.3cm with PHS and 9.6cm with SMS over the three-year simulations. Root zone soil potential is lower with SMS, with a root-fraction-weighted average soil potential of -0.42 MPa during November 2003. The equivalent metric from PHS, average predawn root water potential, is -0.08 MPa.

Under 60% through-fall exclusion, the change in soil water is -1.12 meters with PHS and -0.94 meters with SMS, relative to the ambient simulations (Supp Fig A.9).

With SMS, root-fraction-weighted average soil potential is -2.18MPa during November 2003, whereas PHS average predawn root water potential is -0.37MPa (Figure 11). Observations of root-zone potential based on gravity-corrected predawn leaf water potential are -0.17 ± 0.10 MPa under ambient conditions, and -0.71 ± 0.31 MPa with through-fall exclusion (also in November 2003) [Fisher *et al.*, 2007]. The SMS root-weighted water potential is 1.81 MPa drier (from a soil water potential perspective) because the SMS continues to extract water from dry layers with high fractions of roots, further drying these layers and decreasing the root-weighted water potential (see Section 6.4). Further, PHS has more access to deep soil water under dry conditions (Fig 8), which mitigates declines in soil potential near the surface.

While PHS better matches observations of root-zone soil potential, we hesitate to make conclusions about model skill due to parameter uncertainty and due to the fact that these values may be sensitive to tuning (see Section 4.1), as well as the fact that both models feature high biases in transpiration relative to observations.

Darcy's Law establishes that water flow is proportional to the gradient in total water potential. With PHS, this gradient is measured relative to dynamic ψ_{root} . With SMS, this gradient is measured relative to a constant parameter, ψ_c , the soil water potential at which

784 stomates fully close. This approach is required without prognostic vegetation water potential,
 785 but yields unsatisfactory dynamics that do not comply with the physics of porous media flow
 786 (see Section 6.4). Furthermore, it seems that ψ_c has historically been tuned for its effects
 787 on diffusive fluxes, without specific attention to the effect on soil moisture dynamics (Can
 788 someone else back me up on this? Is there a way to cite this?).

789 This is problematic because soil moisture dynamics are very sensitive to ψ_c . Root wa-
 790 ter uptake halts when soil potential reaches ψ_c (Section 3), setting an effective minimum soil
 791 potential, a situation that is apparent in Figure 11 where soil water potential for SMS stays at
 792 approximately -2.5 MPa, which is the value of ψ_c for evergreen tropical broadleaf trees (?).
 793 This feature is clearer in Figure A.11, where soil layers can be seen to dry out quickly, but
 794 not beyond -2.5 MPa (with the exception of Soil Layers 1 and 2, which are influenced by bare
 795 soil evaporation). The effect of ψ_c extends to ambient through-fall conditions (Fig A.10), but
 796 over a smaller spatial and temporal domain. PHS has more flexibility, due to dynamic root
 797 water potential, so there is not the same tendency to dry out quickly to a specific level. In-
 798 stead minimum soil water potential for PHS gets lower each dry season throughout the TFE
 799 simulation (Fig 11a).

800 [Add some material looking at the vertical profile of soil moisture in the models vs
 801 observations?]

802 Soil water dynamics in CLM are sensitive to the representation of root water uptake,
 803 but due to the scarcity of observational constraints, vertically-resolved soil moisture predic-
 804 tions are challenging to evaluate.

805 With PHS, because we're modeling vegetation water potential, we can utilize a hy-
 806draulic framework, which offers a well-established physical basis and a clear improvement
 807 in model structure. SMS root water uptake has problematic model structure, seemingly no
 808 empirical basis, and intuitively does not look good on soil water dynamics. PHS improves
 809 model structure, but it also adds parameters that are difficult to constrain.

810 PHS offers leaf and stem water potential observations, which are downstream of soil
 811 potential, and could be an exciting opportunity to interface with observations. While PHS
 812 seems a clear improvement over SMS, which does not comport well with fundamental as-
 813 pects of hydraulic theory, further work on the representation of root water uptake in models
 814 is needed to validate both soil water states and fluxes.

815 7 Conclusion

816 7.1 Caveats

817 Modeling stomatal conductance and photosynthesis, especially subject to water stress,
 818 is an area of ongoing research. We use the Medlyn model coupled to a hydraulic stress func-
 819 tion that attenuates V_{cmax} . This complies with observations [Lin et al., 2018; Zhou et al.,
 820 2013] that stress applied through g_1 underestimates attenuation of photosynthesis. However,
 821 there is no direct evidence of declines in V_{cmax} with drought [Flexas et al., 2006], whereby
 822 future work may seek to represent mesophyll conductance in CLM.

823 The model hydraulic supply representation is simplified, to reduce the model parameter
 824 and computational burdens. No capacitance. No integration of xylem or soil conductances
 825 vulnerability, instead based on lower node. No hysteresis in loss of conductance, xylem in-
 826 stantly regain conductance upon re-wetting. Leaf conductance simplified. Soil layers fully
 827 parallel, soil potential constant each time step.

828 Parameter uncertainty is significant. Notions of hydraulic architecture will never per-
 829 fectly fit on this modeling scale, especially in a PFT paradigm. Field measurements of hy-
 830draulic traits will help constrain parameter ranges, but mostly only aboveground. Flux ob-
 831 servations can help to tune stress parameters. Parameter estimation for root functioning is

significantly more challenging, given the difficulty in underground trait observations. Likewise observational constraints of vertically-resolved states and fluxes underground are scarce. Follow-up work will be geared towards parameter estimation and assessing model skill.

7.2 Utility of modeling vegetation water potential

The PHS configuration of the CLM5 is, to our knowledge, the first Earth System Model with a representation of plant water potential running in its default configuration. In this paper, we have described the model implementation, and illustrated a comparison of the model dynamics for a tropical rainforest site subjected to water limitation, given that prediction of rainforest responses to drought is one of the key uncertainties in the ESM predictions. Overall, the new model behaviour differs from the default configuration in ways that are expected, given its structural properties, and in many cases, provides better correspondance with the observations than the default structure.

In this paper, however, we do not undertake a comprehensive assessment of which model structure performs better, given the substantial parametric uncertainty in both models, and the dependence on numerous other features of the CLM external to water stress representation that contribute to model-observation divergences - in this case in particular, the overestimation of unstressed transpiration by both versions of the model compared to the observations.

In lieu of this type of assessment, we propose that the new PHS model structure 1) is more closely aligned with known plant hydraulics theory, 2) provides significantly improved connections to real-world observational data streams (of leaf and stem water status, sap flow, percent loss conductance) and 3) represents known features of ecohydrological function that the default model cannot capture, including hydraulic redistribution, changes in the depth of water uptake with drought stress, plant embolism impacts on gas exchange and responses of water uptake to changes in leaf:root ratios.

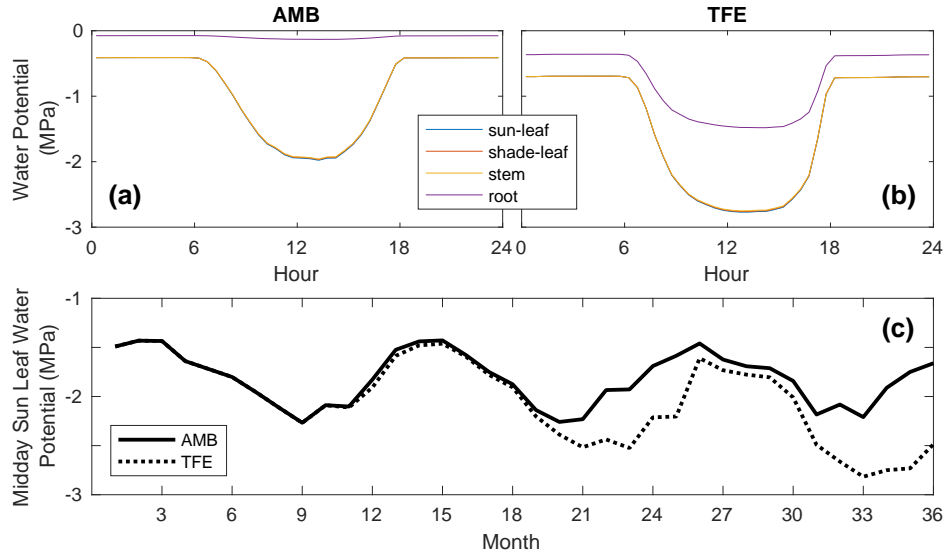
This will be the final conclusions. Any comments on overall takeaways?

PHS models vegetation water potential. This offers structural improvements for stress and for root water uptake. Stress now functions with hydraulic limitation.

8 Acknowledgments

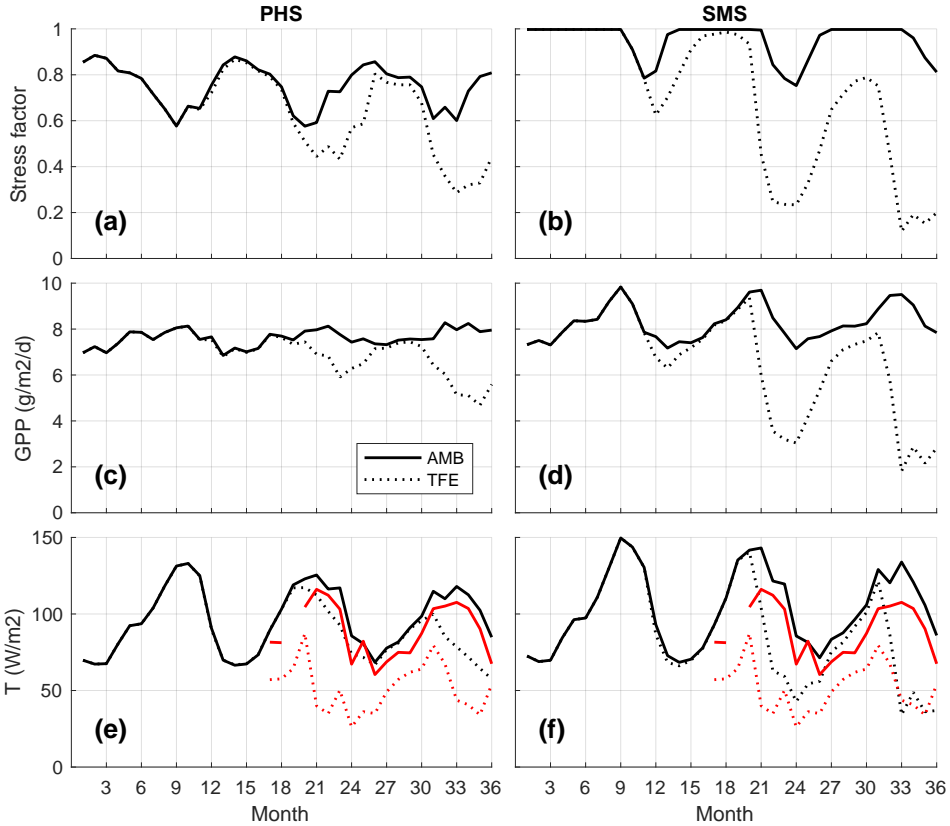
861

9 Figures



862
863
864
865
866
867

Figure 2. Modeled vegetation water potential at Caxiuanã, Brazil. (a) 2003 Dry season (SON) diurnal mean, ambient through-fall conditions, (b) 2003 Dry season (SON) diurnal mean, with 60% through-fall excluded. Curves are drawn for sunlit leaf, shaded leaf, stem, and root water potentials. Note that the first three mostly overlap. (c) Monthly mean midday leaf water potential, under ambient (solid line) and 60% through-fall exclusion (dotted line) conditions. Note that through-fall exclusion begins in month 11 (Nov 1, 2001).



868 **Figure 3.** (a,b) Monthly mean water stress function. Note that the water stress function equals 1 when
 869 there is no stress and 0 when fully stressed. (c,d) Monthly mean transpiration (W/m^2). (e,f) Monthly mean
 870 gross primary productivity ($\text{g}/\text{m}^2/\text{d}$). Solid lines correspond to ambient through-fall conditions, and dotted
 871 lines feature 60% through-fall exclusion. Black lines represent model output. Red lines show observational
 872 transpiration derived from sap flux (see zqz). PHS is on for (a), (c), and (e). PHS is off for (b), (d), and (f).

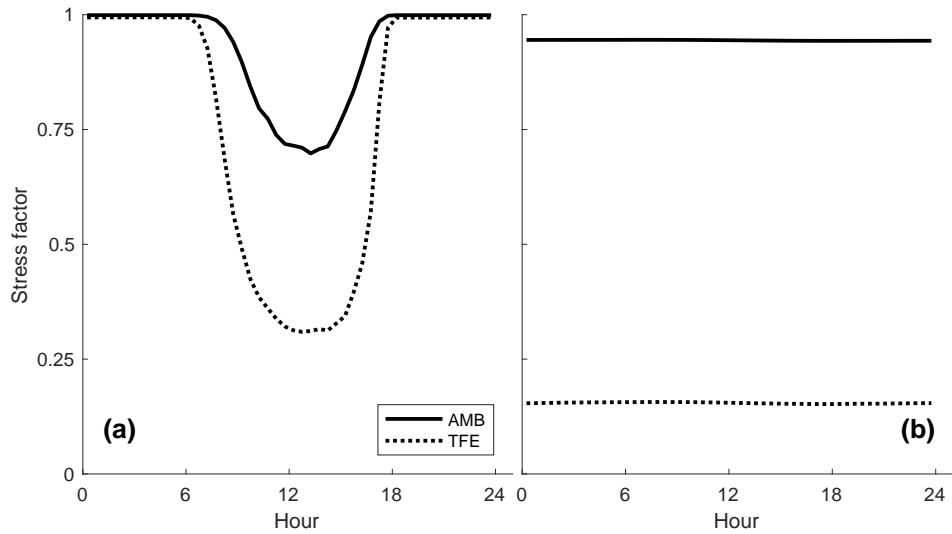
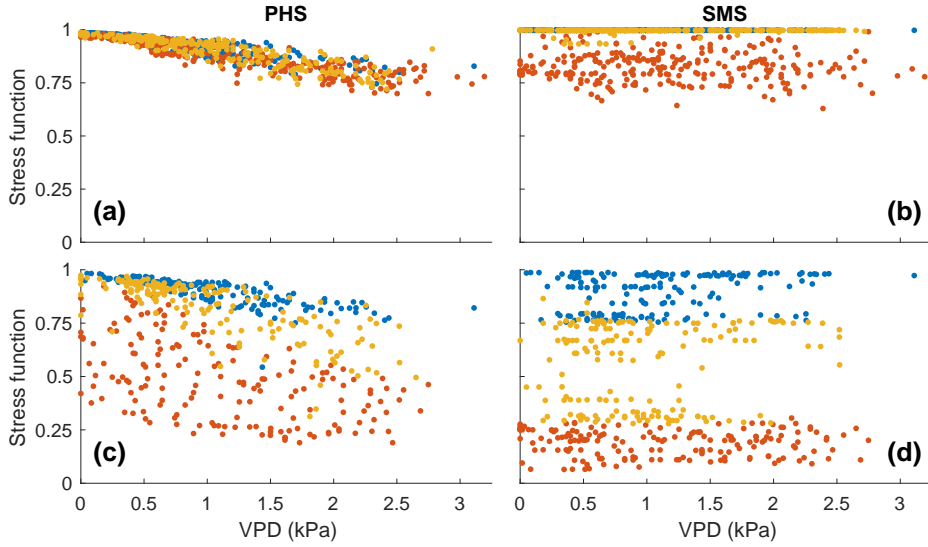


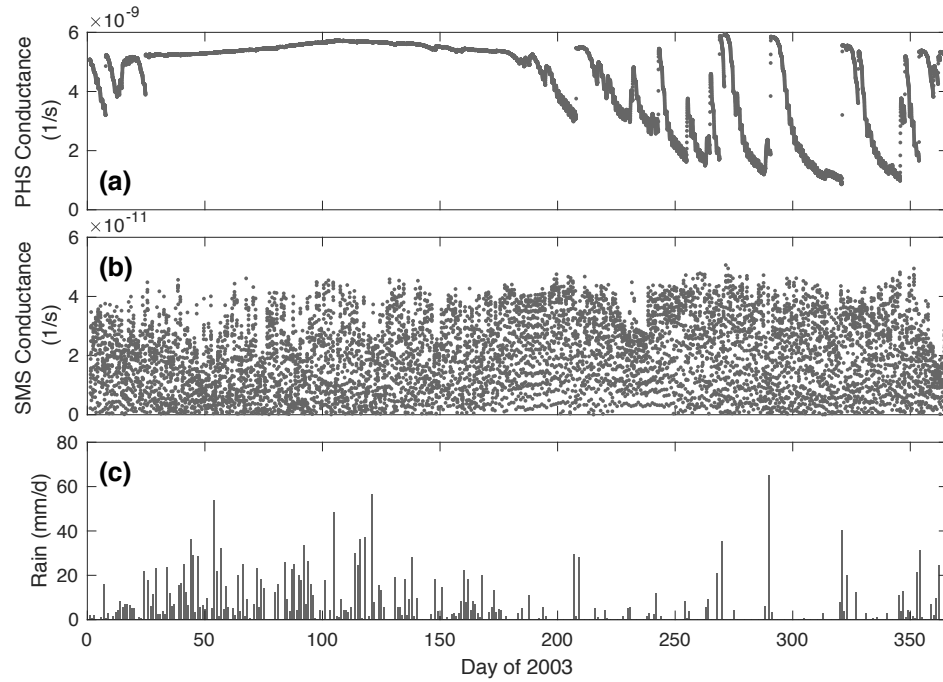
Figure 4. 2003 Dry season (SON) diurnal mean water stress function for (a) PHS on, and (b) PHS off.

Solid lines correspond to ambient through-fall conditions, and dotted lines feature 60% through-fall exclusion.

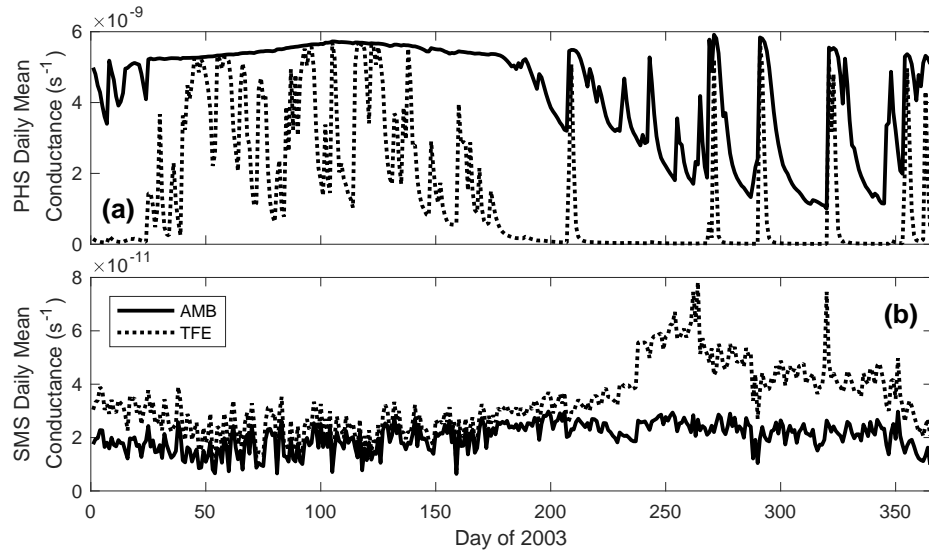
Note that the water stress function equals 1 when there is no stress and 0 when fully stressed.



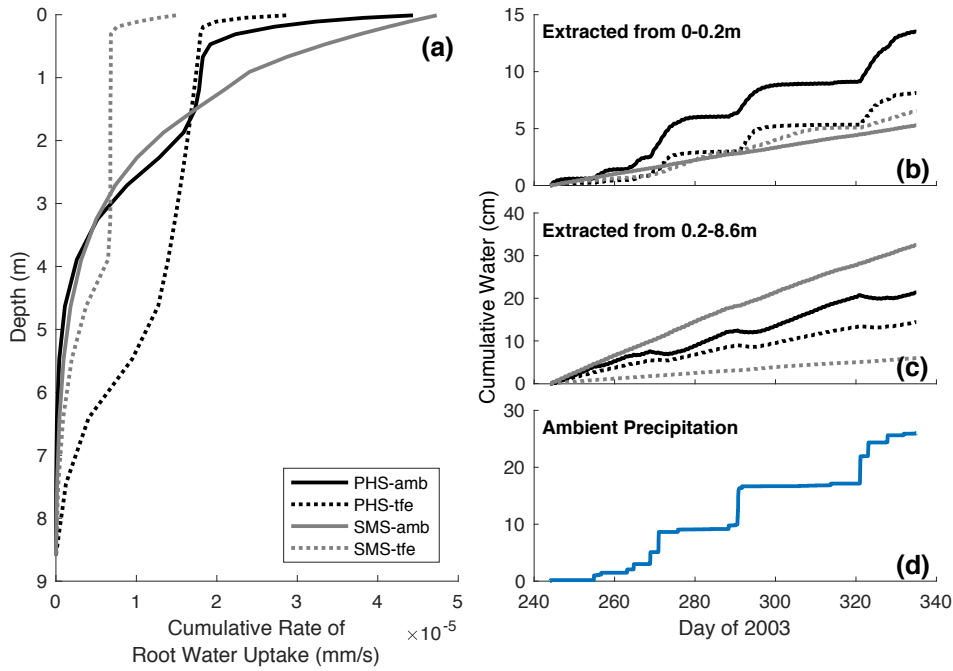
876 **Figure 5.** Water stress function versus vapor pressure deficit, for points with downwelling shortwave radia-
 877 tion between 400 and 425 W/m². (a) PHS, ambient through-fall (b) SMS, ambient through-fall (c) PHS,
 878 60% through-fall excluded (d) SMS, 60% through-fall excluded. For (a) and (c) data are subdivided based
 879 on predawn root water potential. For (b) and (d) data are subdivided based on average soil matric potential,
 880 weighted by root fraction. Blue dots represent the wettest tercile, yellow dots represent the intermediate ter-
 881 cile, and red dots represent the driest tercile. Note that panels (c) and (d) exclude data from 2001, when CO₂
 882 exclusion was not active.



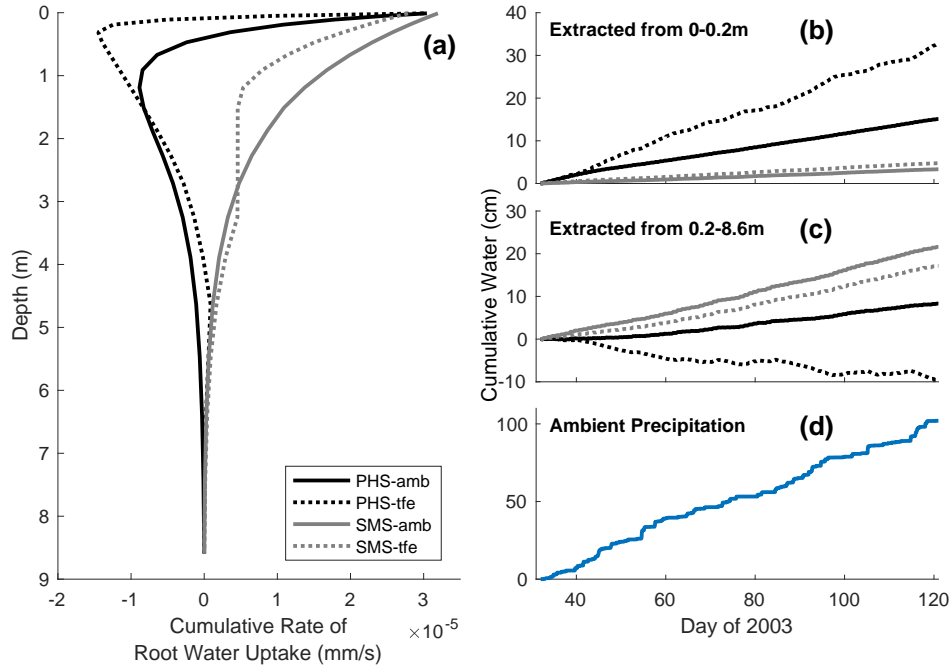
883 **Figure 6.** Soil Layer 3 conductance, under ambient through-fall conditions in 2003. (a) Time-series of
884 PHS modeled soil-to-root conductance (s^{-1}) from Soil Layer 3 (spanning 6 to 12 centimeters in depth). (b)
885 Time-series of SMS inferred conductance (s^{-1}) also from Soil Layer 3. (c) Concurrent precipitation forcing
886 (mm/d).



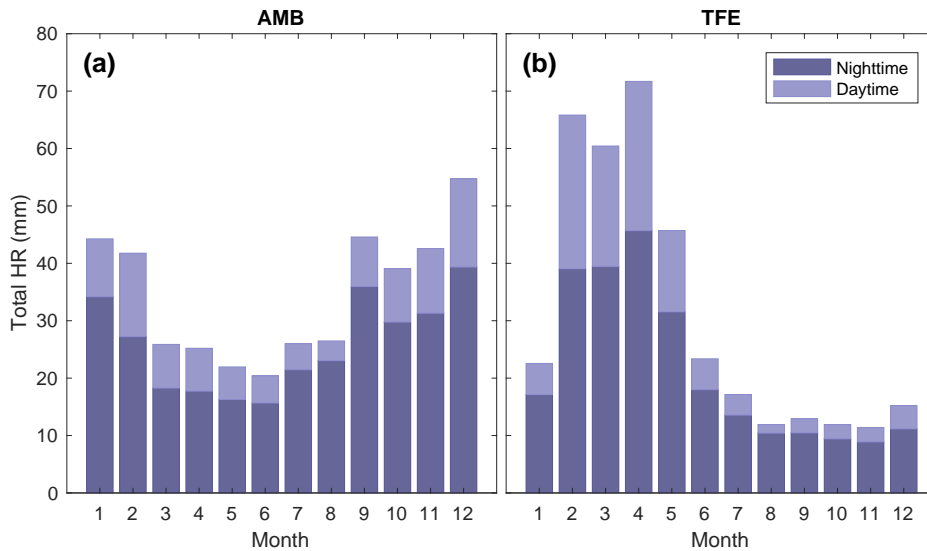
887 **Figure 7.** Daily mean Soil Layer 3 conductance, throughout 2003 under ambient (solid line) and 60%
888 through-fall exclusion (dotted line) conditions. (a) Daily mean of PHS modeled soil-to-root conductance (s^{-1})
889 from Soil Layer 3 (spanning 6 to 12 centimeters in depth). (b) Daily mean of SMS inferred conductance (s^{-1})
890 also from Soil Layer 3.



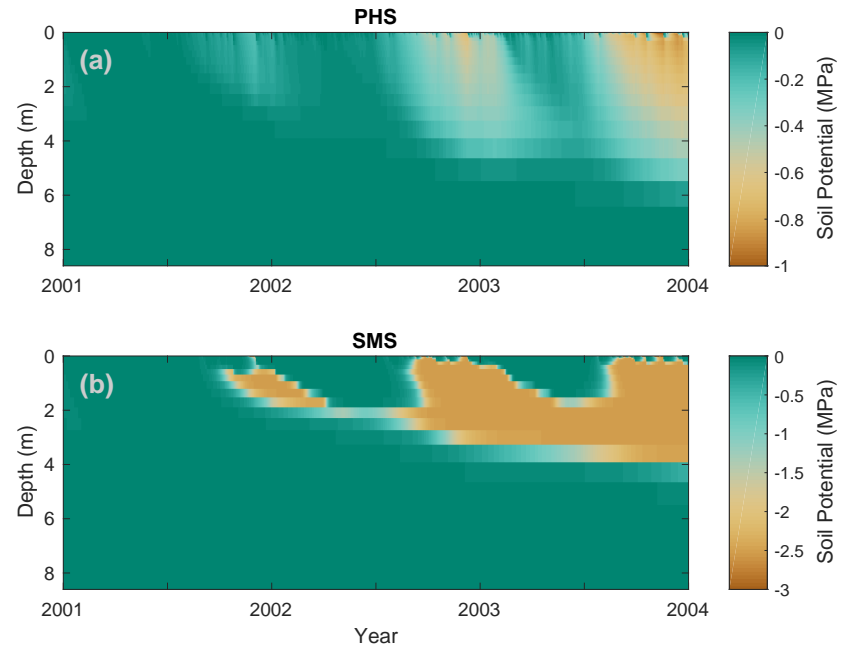
891 **Figure 8.** 2003 dry season (SON) root water uptake. Panel (a) shows the average cumulative profile of root
892 water uptake rate (mm/s) for the four simulations over SON-2003. Panel (b) shows cumulative total water
893 uptake from above 0.2m for the four simulations during SON-2003. Panel (c) shows cumulative total water
894 uptake from below 0.2m for the four simulations during SON-2003. Panel (d) shows cumulative total ambient
895 precipitation during SON-2003.



896 **Figure 9.** 2003 wet season (FMA) root water uptake. Panel (a) shows the average cumulative profile of root
897 water uptake rate (mm/s) for the four simulations over FMA-2003. Panel (b) shows cumulative total water
898 uptake from above 0.2m for the four simulations during FMA-2003. Panel (c) shows cumulative total water
899 uptake from below 0.2m for the four simulations during FMA-2003. Panel (d) shows cumulative total ambient
900 precipitation during FMA-2003.

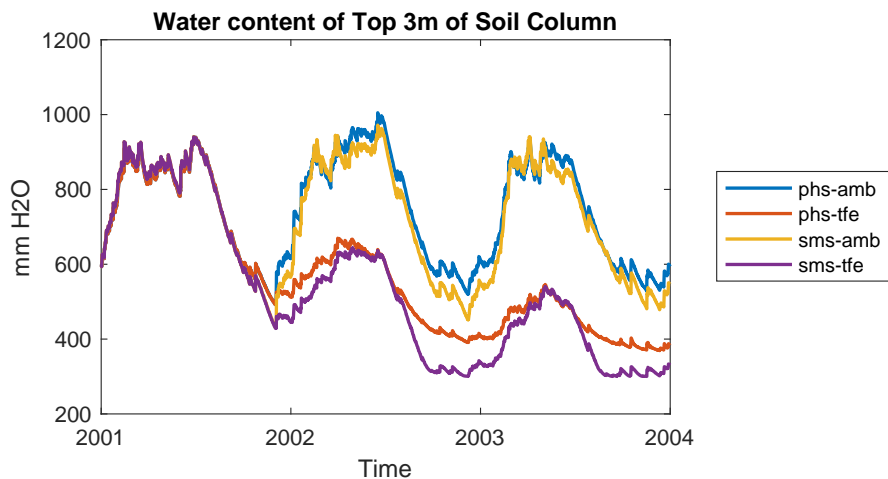


901 **Figure 10.** Total hydraulic redistribution (mm) by month in 2003. For (a) ambient through-fall conditions,
902 and (b) 60% through-fall exclusion. Darker shading shows portion of HR at night [6pm,6am], lighter shading
903 shows portion of HR during day [6am,6pm].

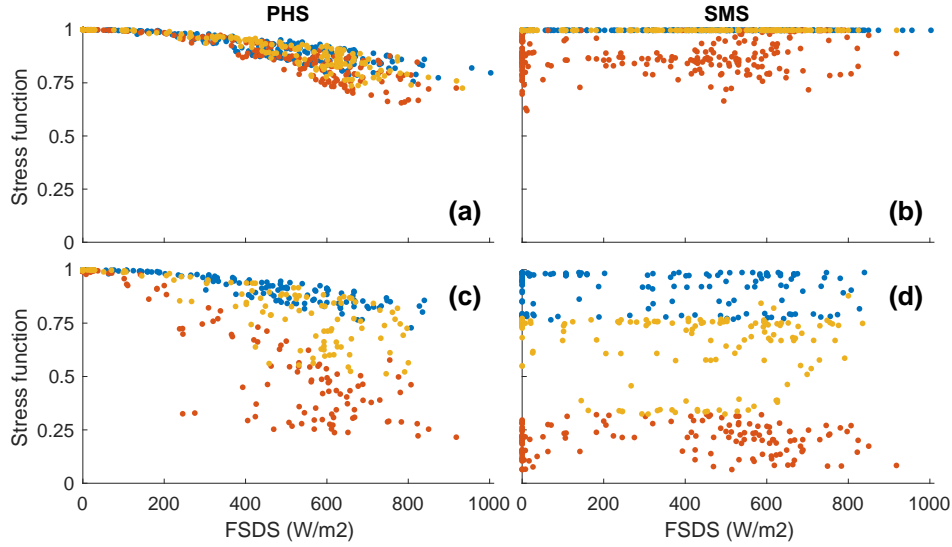


904 **Figure 11.** Vertical profile of soil water potential (MPa) over time under 60% through-fall exclusion, for (a)
905 PHS, and (b) SMS. Note that color axes are different.

906 **A: Supplementary Figures**



907 **Figure A.1.** Total water content of the top three meters of the soil column through time for the four simula-
908 tions.



909 **Figure A.2.** Water stress function versus downwelling shortwave radiation for points with vapor pressure
 910 deficit between 1 and 1.0559 kPa. (a) PHS, ambient through-fall (b) SMS, ambient through-fall (c) PHS,
 911 60% through-fall excluded (d) SMS, 60% through-fall excluded. For (a) and (c) data are subdivided based
 912 on predawn root water potential. For (b) and (d) data are subdivided based on average soil matric potential,
 913 weighted by root fraction. Blue dots represent the wettest tercile, yellow dots represent the intermediate
 914 tercile, and red dots represent the driest tercile. Note that panels (c) and (d) exclude data from 2001, when
 915 through-fall exclusion was not active.

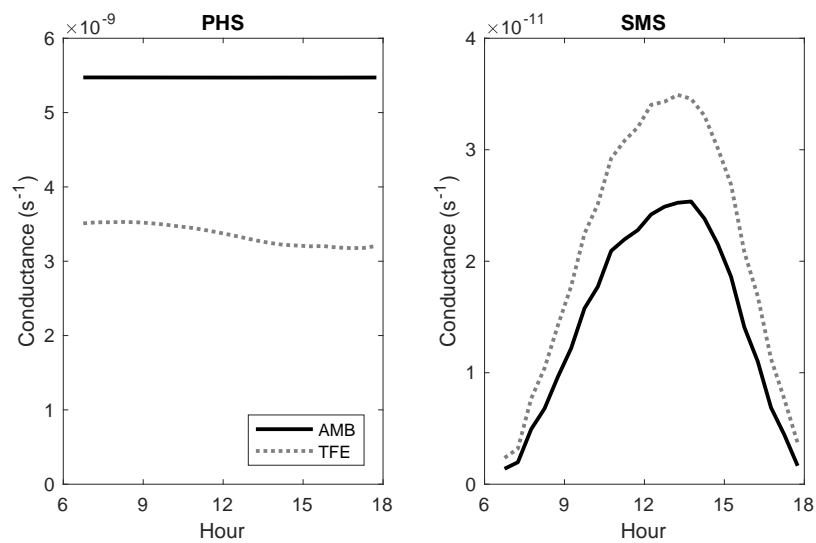


Figure A.3. FMA-2003 average diurnal cycle of layer 3 conductance.

916

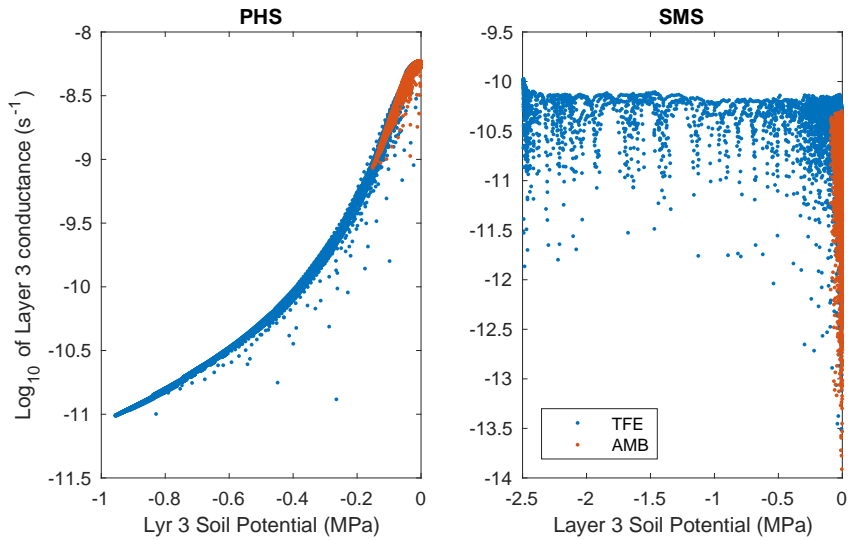


Figure A.4. Log of conductance versus soil potential for Soil Layer 3 (2003).

917

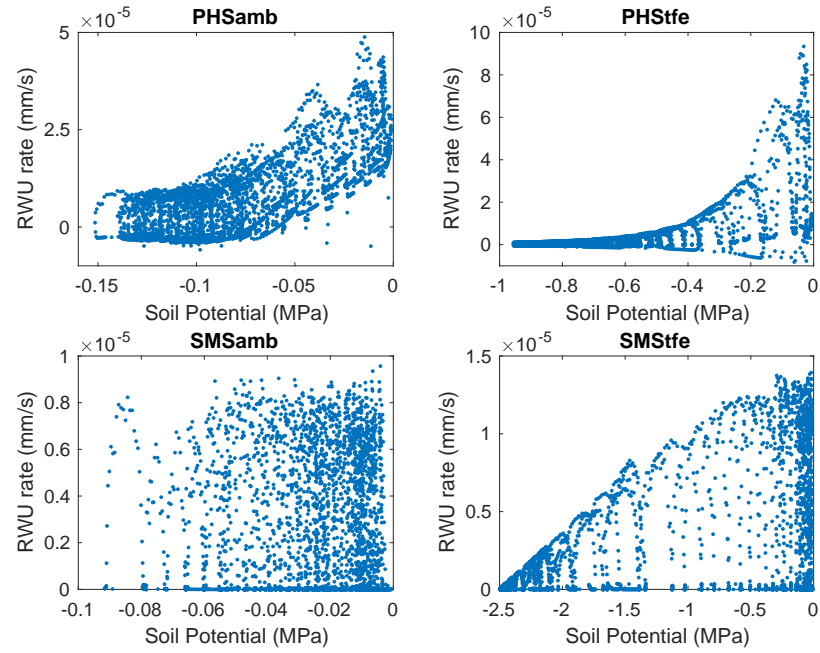
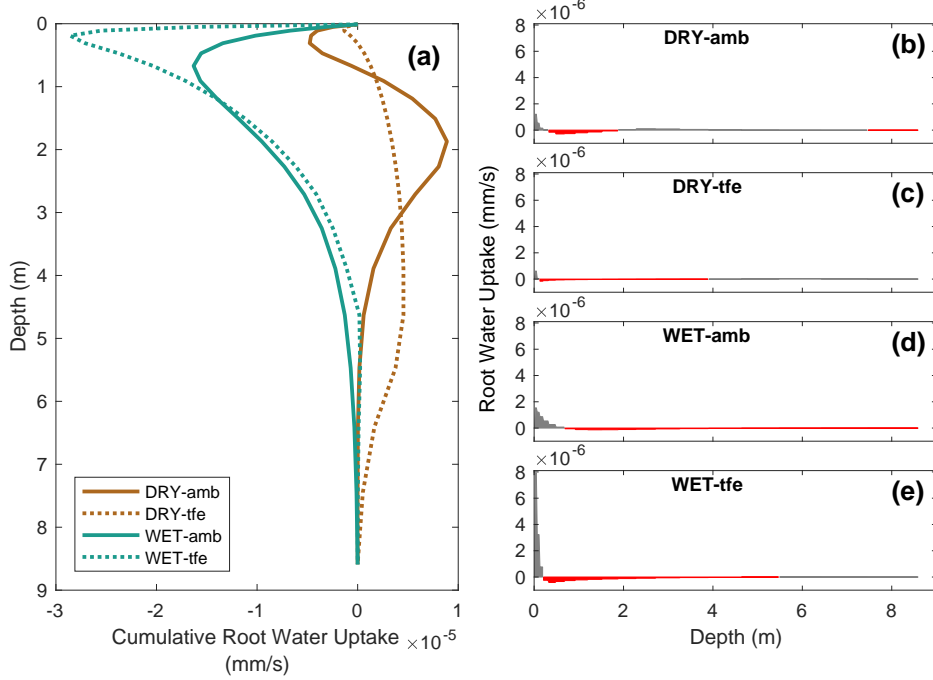
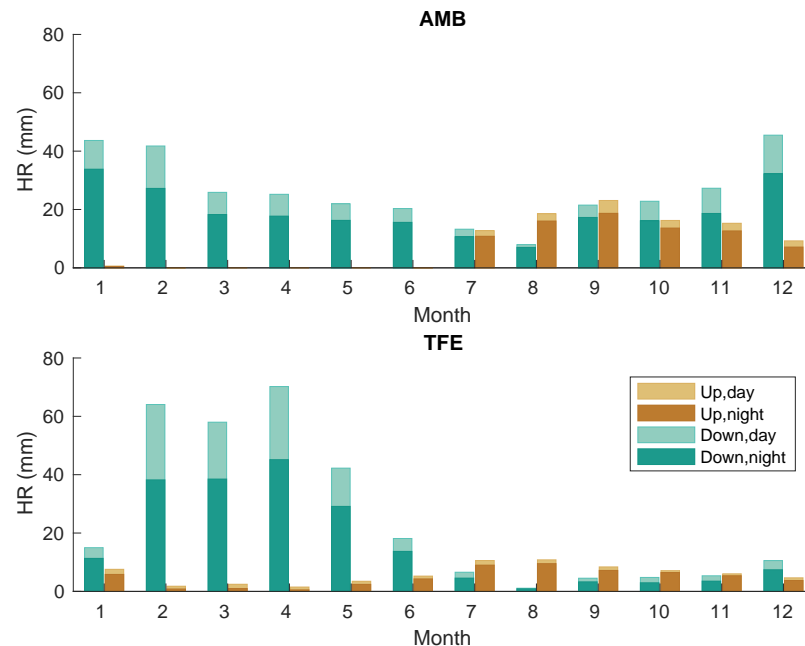


Figure A.5. Root water uptake versus soil potential for Soil Layer 3 (SON-2003).

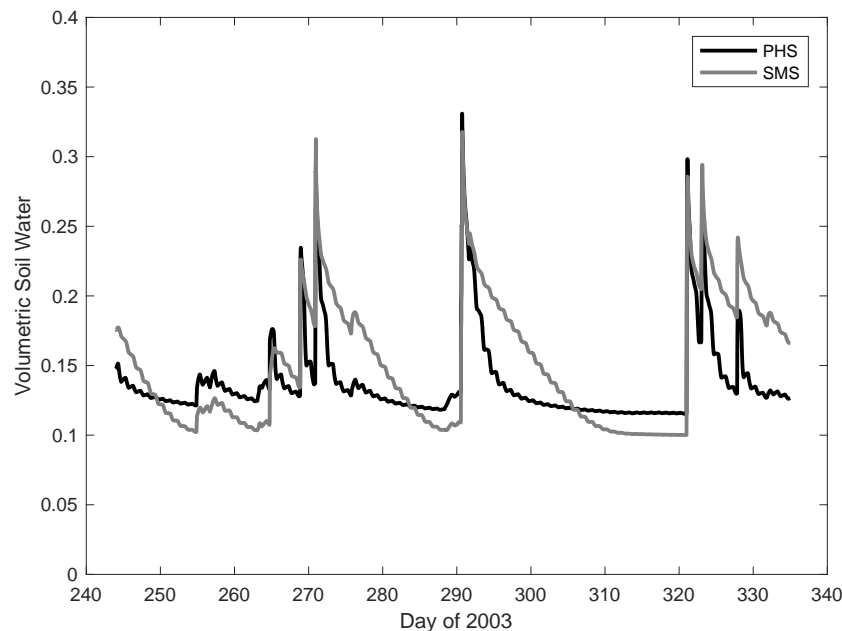


919 **Figure A.6.** PHS, nighttime (6pm to 6am) average root water uptake profiles with depth. Showing night-
 920 time serves to emphasize the profile of hydraulic redistribution. Panel (a) shows cumulative (starting at depth)
 921 root water uptake (mm/s) for ambient (solid line) and 60% through-fall exclusion (dotted line) during the wet
 922 (FMA, cyan color) and dry (SON, brown color) seasons. Panels (b)-(e) present the information from (a) in
 923 non-cumulative form. Note that for panels (b)-(e) negative root water uptake is shaded red, and also that for
 924 panel (a), positive slope indicates water uptake, and negative slope indicates water deposited. Note also that
 925 SMS is not shown, because hydraulic redistribution is precluded.



926

Figure A.7. PHS hydraulic distribution during 2003. Alternative version partitioning by direction.



927 **Figure A.8.** Volumetric soil water content in Soil Layer 2 (which spans 2-6cm in depth), for SON-2003,
928 featuring 60% through-fall exclusion. With PHS (black line), the soil layer can dry out much more quickly
929 after rain events.

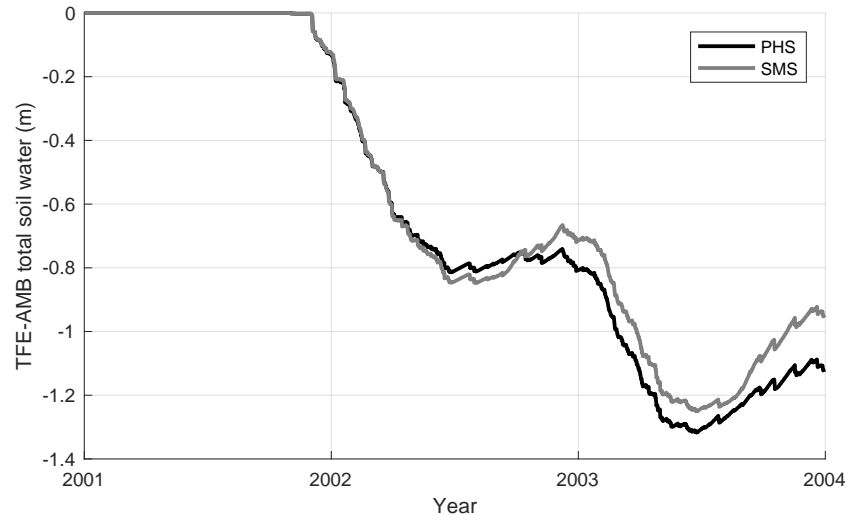
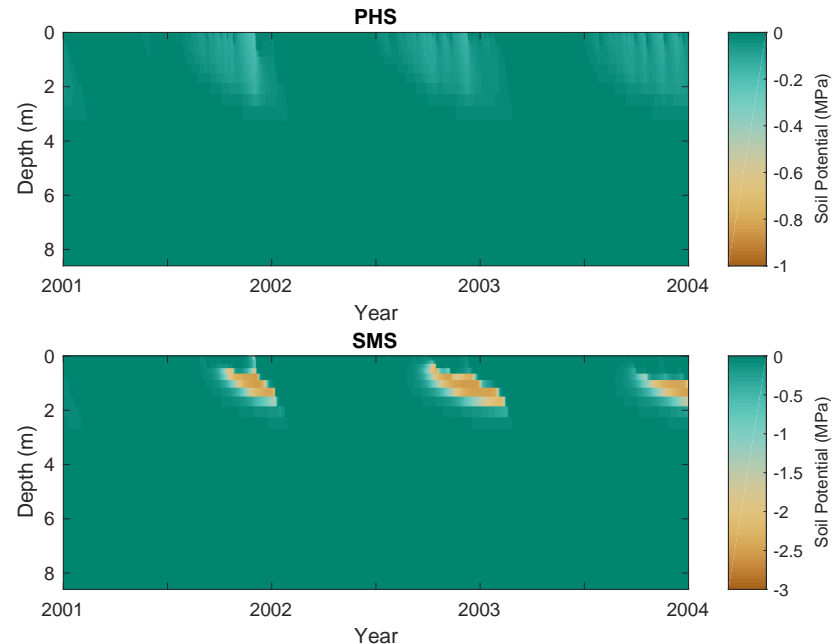
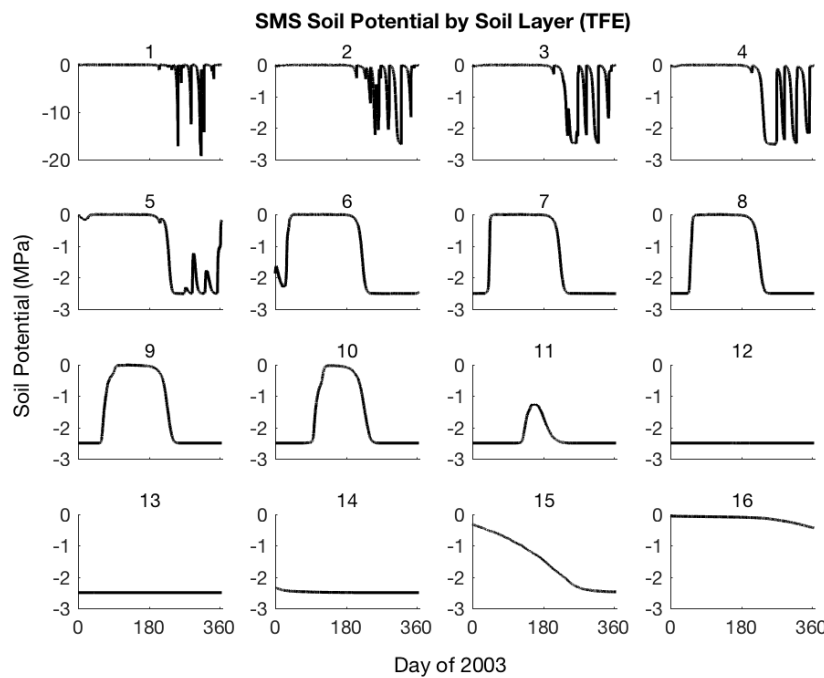


Figure A.9. Delta soil water

930



931 **Figure A.10.** Vertical profile of soil water potential (MPa) through time under ambient through-fall condi-
932 tions, for (a) PHS, and (b) SMS. Note that color axes are different.



933 **Figure A.11.** Time series of soil potential by soil layer, with SMS, under 60% through-fall exclusion. This
 934 duplicates the information in Figure 11a to highlight the the sensitivity of soil moisture dynamics to the SMS
 935 parameter, ψ_c (soil potential with stomates fully closed, -2.5 MPa). Soil Layers 17-20, which do not dry out
 936 completely (similar to Soil Layer 16), are not shown.

937 B: Appendix to Model Description

938 B.1 Details of Water Supply

939 PHS resolves flow across four different segments, soil-to-root, root-to-stem, stem-to-
 940 leaf, and leaf-to-transpiration.

941 Stem-to-leaf. The area bases are sunlit and shaded leaf area, respectively. Note that
 942 gravity is assumed negligible here. Likewise there is no length scaling applied to maximum
 943 conductance. Therefore the input parameters for $k_{1,\max}$ should be conductances (s^{-1}).

$$944 \begin{aligned} q_{1a} &= k_1 \cdot \text{LAI-sun} \cdot (\psi_{\text{stem}} - \psi_{\text{sun-leaf}}) \\ q_{1b} &= k_1 \cdot \text{LAI-shade} \cdot (\psi_{\text{stem}} - \psi_{\text{shade-leaf}}) \end{aligned} \quad (B.1)$$

$$945 k_1 = k_{1,\max} \cdot f(\psi_{\text{stem}}) \quad (B.2)$$

$$946 f(\psi) = 2^{-\left(\frac{\psi}{p_{50}}\right)^{c_k}} \quad (B.3)$$

947 Root-to-stem. The area basis is stem area index. The parameter is maximum stem
 948 xylem conductivity ($K_{2,\max}$). Stem conductance (k_2) is the result of scaling maximum con-
 949 ductivity by the tree height (h) and applying loss relative to maximum conductance via the
 950 vulnerability curve $f(\psi_{\text{root}})$.

$$951 q_2 = k_2 \cdot \text{SAI} \cdot (\psi_{\text{root}} - \psi_{\text{stem}} - \rho g h) \quad (B.4)$$

$$952 k_2 = \frac{K_{2,\max}}{h} \cdot f(\psi_{\text{root}}) \quad (B.5)$$

953 Soil-to-root. Area basis is RAI in soil layer i , which is based on the layer root fraction
 954 times the total root area. Total root area we have as the summed stem and leaf area indices
 955 multiplied by a relative root area parameter (f_{root}). The vertical root distribution is defined
 956 by the layer root fraction (r_i), which follows a one-parameter (by PFT) power law decay fol-
 957 lowing Jackson *et al.* [1996].

$$959 q_{3,i} = k_{3,i} \cdot \text{RAI}_i \cdot (\psi_{\text{soil},i} - \psi_{\text{root}} - \rho g z_i) \quad (B.6)$$

$$960 \text{RAI}_i = f_{\text{root}} \cdot (\text{SAI} + \text{LAI}) \cdot r_i \quad (B.7)$$

$$961 k_{3,i} = \frac{k_{r,i} + k_{s,i}}{k_{r,i} \cdot k_{s,i}} \quad (B.8)$$

$$962 k_{r,i} = \frac{K_{r,\max}}{l_i} f(\psi_{\text{soil},i}) \quad (B.9)$$

$$963 l_i = z_i + x \quad (B.10)$$

$$964 k_{s,i} = \frac{K_{s,i}}{d} \quad (B.11)$$

965 The conductance $k_{3,i}$ reflects two resistors in series, from soil-to-root ($k_{s,i}$) and through
 966 the root tissue ($k_{r,i}$). The root tissue conductance is attenuated via the vulnerability curve
 967 framework. The input parameter is maximum root xylem conductivity, on the basis of RAI
 968 as defined above. The root conductivity is scaled by the conducting length, which is esti-
 969 mated as the sum of soil layer depth (z_i) and average lateral extent (x , static parameter). The
 970 soil conductivity $K_{s,i}$ is calculated from the layer soil matric potential (ψ_s) and soil proper-
 971 ties following Clapp and Hornberger [1978] as described in Oleson *et al.* [2013]. The soil
 972 conductance ($k_{s,i}$) is the result of scaling the conductivity by d , the distance between roots
 973 estimated following Williams *et al.* [1996] and Bonan *et al.* [2014].

974 The challenge here is obviously getting your head around all the parameters.
 975

980 **B.2 Details of Water Demand**

981 **B.3 Details of Solution**

982 The continuity of water flow through the system yields four equations

$$\begin{aligned} E_{sun} &= q_{1a} \\ E_{shade} &= q_{1b} \\ q_{1a} + q_{1b} &= q_2 \\ q_2 &= \sum_{i=1}^{nlevsoi} q_{3,i} \end{aligned} \quad (B.12)$$

984 We seek the set of vegetation water potential values (four unknowns),

$$\psi = \begin{bmatrix} \psi_{sunleaf} \\ \psi_{shadeleaf} \\ \psi_{stem} \\ \psi_{root} \end{bmatrix} \quad (B.13)$$

986 that satisfies these equations, as forced by the soil moisture and atmospheric state.

987 Each flux on the schematic can be represented in terms of the relevant water potentials.

988 Defining the transpiration fluxes:

$$\begin{aligned} E_{sun} &= E_{sun,max} \cdot 2^{-\left(\frac{\psi_{sunleaf}}{p50_e}\right)^{c_k}} \\ E_{shade} &= E_{shade,max} \cdot 2^{-\left(\frac{\psi_{shadeleaf}}{p50_e}\right)^{c_k}} \end{aligned} \quad (B.14)$$

990 Defining the water supply fluxes:

$$\begin{aligned} q_{1a} &= k_{1a,max} \cdot 2^{-\left(\frac{\psi_{stem}}{p50_1}\right)^{c_k}} \cdot LAI_{sun} \cdot (\psi_{stem} - \psi_{sunleaf}) \\ q_{1b} &= k_{1b,max} \cdot 2^{-\left(\frac{\psi_{stem}}{p50_1}\right)^{c_k}} \cdot LAI_{shade} \cdot (\psi_{stem} - \psi_{shadeleaf}) \\ q_2 &= \frac{k_{2,max}}{z_2} \cdot 2^{-\left(\frac{\psi_{root}}{p50_2}\right)^{c_k}} \cdot SAI \cdot (\psi_{root} - \psi_{stem} - \Delta\psi_z) \\ q_{soil} &= \sum_{i=1}^{nlevsoi} q_{3,i} = \sum_{i=1}^{nlevsoi} k_{3,i} \cdot RAI \cdot (\psi_{soil,i} - \psi_{root} + \Delta\psi_{z,i}) \end{aligned} \quad (B.15)$$

992 We're looking to find the vector ψ that fits with soil and atmospheric forcings while
 993 satisfying water flow continuity. Due to the model non-linearity, we use a linearized explicit
 994 approach, iterating with Newton's method. The initial guess is the solution for ψ (vector)
 995 from the previous time step. The general framework, from iteration m to $m + 1$ is:

$$\begin{aligned} q^{m+1} &= q^m + \frac{\delta q}{\delta \psi} \Delta \psi \\ \psi^{m+1} &= \psi^m + \Delta \psi \end{aligned} \quad (B.16)$$

997 So for our first flux balance equation, at iteration $m + 1$, we have:

998

$$E_{sun}^{m+1} = q_{1a}^{m+1} \quad (\text{B.17})$$

999

Which can be linearized to:

1000

$$E_{sun}^m + \frac{\delta E_{sun}}{\delta \psi} \Delta \psi = q_{1a}^m + \frac{\delta q_{1a}}{\delta \psi} \Delta \psi \quad (\text{B.18})$$

1001

And rearranged to be:

1002

$$\frac{\delta q_{1a}}{\delta \psi} \Delta \psi - \frac{\delta E_{sun}}{\delta \psi} \Delta \psi = E_{sun}^m - q_{1a}^m \quad (\text{B.19})$$

1003

And for the other 3 flux balance equations:

1004

$$\begin{aligned} \frac{\delta q_{1b}}{\delta \psi} \Delta \psi - \frac{\delta E_{sha}}{\delta \psi} \Delta \psi &= E_{sha}^m - q_{1b}^m \\ \frac{\delta q_2}{\delta \psi} \Delta \psi - \frac{\delta q_{1a}}{\delta \psi} \Delta \psi - \frac{\delta q_{1b}}{\delta \psi} \Delta \psi &= q_{1a}^m + q_{1b}^m - q_2^m \\ \frac{\delta q_{soil}}{\delta \psi} \Delta \psi - \frac{\delta q_2}{\delta \psi} \Delta \psi &= q_2^m - q_{soil}^m \end{aligned} \quad (\text{B.20})$$

1005

Putting all four together in matrix form:

1006

$$\begin{bmatrix} \frac{\delta q_{1a}}{\delta \psi} - \frac{\delta E_{sun}}{\delta \psi} \\ \frac{\delta q_{1b}}{\delta \psi} - \frac{\delta E_{sha}}{\delta \psi} \\ \frac{\delta q_2}{\delta \psi} - \frac{\delta q_{1a}}{\delta \psi} - \frac{\delta q_{1b}}{\delta \psi} \\ \frac{\delta q_{soil}}{\delta \psi} - \frac{\delta q_2}{\delta \psi} \end{bmatrix} \Delta \psi = \begin{bmatrix} E_{sun}^m - q_{1a}^m \\ E_{sha}^m - q_{1b}^m \\ q_{1a}^m + q_{1b}^m - q_2^m \\ q_2^m - q_{soil}^m \end{bmatrix} \quad (\text{B.21})$$

1007

1008

Now to expand the left-hand side, from vector ψ to the four distinct plant water potential nodes, noting that many derivatives are zero (e.g. $\frac{\delta E_{sun}}{\delta \psi_{sha}} = 0$)

1009

Introducing the notation: $A \Delta \psi = b$

1010

$$\Delta \psi = \begin{bmatrix} \Delta \psi_{sunleaf} \\ \Delta \psi_{shadeleaf} \\ \Delta \psi_{stem} \\ \Delta \psi_{root} \end{bmatrix} \quad (\text{B.22})$$

$$A = \begin{bmatrix} \frac{\delta q_{1a}}{\delta \psi_{sun}} - \frac{\delta E_{sun}}{\delta \psi_{sun}} & 0 & \frac{\delta q_{1a}}{\delta \psi_{stem}} & 0 \\ 0 & \frac{\delta q_{1b}}{\delta \psi_{sha}} - \frac{\delta E_{sha}}{\delta \psi_{sha}} & \frac{\delta q_{1b}}{\delta \psi_{stem}} & 0 \\ -\frac{\delta q_{1a}}{\delta \psi_{sun}} & -\frac{\delta q_{1b}}{\delta \psi_{sha}} & \frac{\delta q_2}{\delta \psi_{stem}} - \frac{\delta q_{1a}}{\delta \psi_{stem}} - \frac{\delta q_{1b}}{\delta \psi_{stem}} & \frac{\delta q_2}{\delta \psi_{root}} \\ 0 & 0 & -\frac{\delta q_2}{\delta \psi_{stem}} & \frac{\delta q_{soil}}{\delta \psi_{root}} - \frac{\delta q_2}{\delta \psi_{root}} \end{bmatrix} \quad (\text{B.23})$$

1011

$$1012 \quad b = \begin{bmatrix} E_{sun}^m - q_{b1}^m \\ E_{shade}^m - q_{b2}^m \\ q_{b1}^m + q_{b2}^m - q_{stem}^m \\ q_{stem}^m - q_{soil}^m \end{bmatrix} \quad (B.24)$$

1013 Now we compute all the entries for A and b based on the soil moisture and maximum
 1014 transpiration forcings and can solve to find:

$$1015 \quad \Delta\psi = A^{-1}b \quad (B.25)$$

$$1016 \quad \psi_{m+1} = \psi_m + \Delta\psi \quad (B.26)$$

1017 We iterate until $b \rightarrow 0$, signifying water flux balance through the system. The result is
 1018 a final set of water potentials ($\psi_{root}, \psi_{xylem}, \psi_{shadeleaf}, \psi_{sunleaf}$) satisfying non-divergent
 1019 water flux through the system. The magnitude of the water flux is driven by soil matric po-
 1020 tential and unstressed ($\beta_t = 1$) transpiration.

1021 We use the transpiration solution (corresponding to the final solution for ψ) to compute
 1022 stomatal conductance. The stomatal conductance is then used to compute β_t .

$$1023 \quad \beta_{t,sun} = \frac{g_{s,sun}}{g_{s,sun,\beta_t=1}} \quad (B.27)$$

$$1024 \quad \beta_{t,shade} = \frac{g_{s,shade}}{g_{s,shade,\beta_t=1}} \quad (B.28)$$

1025 The β_t values are used in the Photosynthesis module (see section 2.1) to apply water
 1026 stress. The solution for ψ is saved as a new variable (vegetation water potential) and is in-
 1027 dicative of plant water status. The soil-to-root fluxes ($q_{3,1}, q_{3,2}, \dots, q_{3,n}$) are used as the soil
 1028 transpiration sink in the Richards' equation subsurface flow equations.

1029 Furthermore several simplifications were made that decrease the numerical complex-
 1030 ity. For the purposes of the PHS solution, soil potentials are assumed constant during each
 1031 timestep. Plant tissue water storage (capacitance) is not represented, whereby the solution
 1032 does not depend on the previous timestep and has no time derivatives.

1033 Acknowledgments

1034 = enter acknowledgments here =

1035 Pierre: Text I removed While there are disagreements about soil moisture trends glob-
 1036 ally [Dai, 2013; Sheffield et al., 2012], Amazonia has experienced and a lengthening dry sea-
 1037 son [Fu et al., 2013] and faces projections of increasing frequency of extreme El Niño events
 1038 [Cai et al., 2014]

1039 References

- 1040 Allen, C. D., A. K. Macalady, H. Chenchouni, D. Bachelet, N. McDowell, M. Vennetier,
 1041 T. Kitzberger, A. Rigling, D. D. Breshears, E. T. Hogg, P. Gonzalez, R. Fensham,
 1042 Z. Zhang, J. Castro, N. Demidova, J.-H. Lim, G. Allard, S. W. Running, A. Semerci, and
 1043 N. Cobb (2010), A global overview of drought and heat-induced tree mortality reveals
 1044 emerging climate change risks for forests, *Forest Ecology and Management*, 259(4), 660 –
 1045 684, doi:<https://doi.org/10.1016/j.foreco.2009.09.001>.

- 1046 Anderegg, W. R. L. (2015a), Spatial and temporal variation in plant hydraulic traits and their
 1047 relevance for climate change impacts on vegetation, *New Phytologist*, 205(3), 1008–1014,
 1048 doi:10.1111/nph.12907.
- 1049 Anderegg, W. R. L., J. M. Kane, and L. D. L. Anderegg (2013a), Consequences of
 1050 widespread tree mortality triggered by drought and temperature stress, *Nature Climate
 1051 Change*, 3(1), 30–36.
- 1052 Anderegg, W. R. L., L. Plavcová, L. D. L. Anderegg, U. G. Hacke, J. A. Berry, and C. B.
 1053 Field (2013b), Drought's legacy: multiyear hydraulic deterioration underlies widespread
 1054 aspen forest die-off and portends increased future risk, *Global Change Biology*, 19(4),
 1055 1188–1196, doi:10.1111/gcb.12100.
- 1056 Anderegg, W. R. L., C. Schwalm, F. Biondi, J. J. Camarero, G. Koch, M. Litvak, K. Ogle,
 1057 J. D. Shaw, E. Shevliakova, A. P. Williams, A. Wolf, E. Ziacon, and S. Pacala (2015b), Per-
 1058 vasive drought legacies in forest ecosystems and their implications for carbon cycle mod-
 1059 els, *Science*, 349(6247), 528–532, doi:10.1126/science.aab1833.
- 1060 Bartlett, M. K., T. Klein, S. Jansen, B. Choat, and L. Sack (2016), The correlations and se-
 1061 quence of plant stomatal, hydraulic, and wilting responses to drought, *Proceedings of the
 1062 National Academy of Sciences*, 113(46), 13,098–13,103, doi:10.1073/pnas.1604088113.
- 1063 Bonan, G. B., P. J. Lawrence, K. W. Oleson, S. Levis, M. Jung, M. Reichstein, D. M.
 1064 Lawrence, and S. C. Swenson (2011), Improving canopy processes in the Commu-
 1065 nity Land Model version 4 (CLM4) using global flux fields empirically inferred from
 1066 FLUXNET data, *Journal of Geophysical Research*, 116, doi:10.1029/2010JG001593.
- 1067 Bonan, G. B., M. Williams, R. A. Fisher, and K. W. Oleson (2014), Modeling stomatal con-
 1068 ductance in the earth system: linking leaf water-use efficiency and water transport along
 1069 the soil-plant-atmosphere continuum, *Geoscientific Model Development*, 7(5), 2193–2222,
 1070 doi:10.5194/gmd-7-2193-2014.
- 1071 Brooks, J. R., F. C. Meinzer, J. M. Warren, J.-C. Domec, and R. Coulombe (2006), Hydraulic
 1072 redistribution in a douglas-fir forest: lessons from system manipulations, *Plant, Cell &
 1073 Environment*, 29(1), 138–150, doi:10.1111/j.1365-3040.2005.01409.x.
- 1074 Burgess, S. S. O., M. A. Adams, N. C. Turner, and C. K. Ong (1998), The redistribution of
 1075 soil water by tree root systems, *Oecologia*, 115(3), 306–311, doi:10.1007/s004420050521.
- 1076 Cai, W., S. Borlace, M. Lengaigne, P. Van Renssch, M. Collins, G. Vecchi, A. Timmermann,
 1077 A. Santoso, M. J. McPhaden, L. Wu, M. H. England, G. Wang, E. Guilyardi, and F.-f. Jin
 1078 (2014), Increasing frequency of extreme El Niño events due to greenhouse warming, *Na-
 1079 ture Climate Change*, 4(2), 111–116.
- 1080 Celia, M. A., E. T. Bouloutas, and R. L. Zarba (1990), A general mass-conservative numer-
 1081 ical solution for the unsaturated flow equation, *Water Resources Research*, 26(7), 1483–
 1082 1496, doi:10.1029/WR026i007p01483.
- 1083 Choat, B., S. Jansen, T. J. Brodribb, H. Cochard, S. Delzon, R. Bhaskar, S. J. Bucci, T. S.
 1084 Feild, S. M. Gleason, U. G. Hacke, A. L. Jacobsen, F. Lens, H. Maherli, J. Martínez-
 1085 Vilalta, S. Mayr, M. Mencuccini, P. J. Mitchell, A. Nardini, J. Pitermann, R. B. Pratt, J. S.
 1086 Sperry, M. Westoby, I. J. Wright, and A. E. Zanne (2012), Global convergence in the vul-
 1087 nerability of forests to drought, *Nature*, 491(7426), 752–5.
- 1088 Christoffersen, B. O., M. Gloor, S. Fauset, N. M. Fyllas, D. R. Galbraith, T. R. Baker,
 1089 B. Kruijt, L. Rowland, R. A. Fisher, O. J. Binks, S. Sevanto, C. Xu, S. Jansen, B. Choat,
 1090 M. Mencuccini, N. G. McDowell, and P. Meir (2016), Linking hydraulic traits to tropi-
 1091 cal forest function in a size-structured and trait-driven model (tsfs v.1-hydro), *Geoscientific
 1092 Model Development*, 9(11), 4227–4255, doi:10.5194/gmd-9-4227-2016.
- 1093 Clapp, R. B., and G. M. Hornberger (1978), Empirical equations for some soil hydraulic
 1094 properties, *Water Resources Research*, 14(4), 601–604, doi:10.1029/WR014i004p00601.
- 1095 Collatz, G., J. Ball, C. Grivet, and J. A. Berry (1991), Physiological and environmental reg-
 1096 ulation of stomatal conductance, photosynthesis and transpiration: a model that includes
 1097 a laminar boundary layer, *Agricultural and Forest Meteorology*, 54(2), 107 – 136, doi:
 1098 http://dx.doi.org/10.1016/0168-1923(91)90002-8.

- 1099 da Costa, A. C., D. B. Metcalfe, C. E. Doughty, A. A. de Oliveira, G. F. Neto, M. C.
 1100 da Costa, J. de Athaydes Silva Junior, L. E. Aragão, S. Almeida, D. R. Galbraith, L. M.
 1101 Rowland, P. Meir, and Y. Malhi (2014), Ecosystem respiration and net primary produc-
 1102 tivity after 8–10 years of experimental through-fall reduction in an eastern Amazon forest,
Plant Ecology & Diversity, 7(1–2), 7–24, doi:10.1080/17550874.2013.798366.
- 1103 da Costa, A. C. L., D. Galbraith, S. Almeida, B. Takeshi, T. Portela, M. da Costa, J. ao de
 1104 Athaydes Silva Junior, A. P. Braga, P. H. L. de Gonçalves, A. A. de Oliveira, R. Fisher,
 1105 O. L. Phillips, D. B. Metcalfe, P. Levy, and P. Meir (2010), Effect of 7 yr of experimental
 1106 drought on vegetation dynamics and biomass storage of an eastern amazonian rainforest,
The New Phytologist, 187(3), 579–591.
- 1107 Dai, A. (2013), Increasing drought under global warming in observations and models, *Nature*
 1108 *Climate Change*, 3(1), 52–58.
- 1109 Dai, Y., R. E. Dickinson, and Y.-P. Wang (2004), A two-big-leaf model for canopy tempera-
 1110 ture, photosynthesis, and stomatal conductance, *Journal of Climate*, 17(12), 2281–2299,
 1111 doi:10.1175/1520-0442(2004)017<2281:ATMFCT>2.0.CO;2.
- 1112 De Kauwe, M. G., J. Kala, Y.-S. Lin, A. J. Pitman, B. E. Medlyn, R. A. Duursma,
 1113 G. Abramowitz, Y.-P. Wang, and D. G. Miralles (2015), A test of an optimal stomatal
 1114 conductance scheme within the CABLE land surface model, *Geoscientific Model Devel-
 1115 opment*, 8(2), 431–452, doi:10.5194/gmd-8-431-2015.
- 1116 De Kauwe, M. G., B. E. Medlyn, J. Knauer, and C. A. Williams (2017), Ideas and perspec-
 1117 tives: how coupled is the vegetation to the boundary layer?, *Biogeosciences*, 14(19), 4435–
 1118 4453, doi:10.5194/bg-14-4435-2017.
- 1119 Domec, J.-C., J. S. King, A. Noormets, E. Treasure, M. J. Gavazzi, G. Sun, and S. G. Mc-
 1120 Nulty (2010), Hydraulic redistribution of soil water by roots affects whole-stand evapo-
 1121 transpiration and net ecosystem carbon exchange, *The New Phytologist*, 187(1), 171–183,
 1122 doi:10.1111/j.1469-8137.2010.03245.x.
- 1123 Drake, J., S. Power, R. Duursma, B. Medlyn, M. Aspinwall, B. Choat, D. Creek, D. Eamus,
 1124 C. Maier, S. Pfautsch, R. Smith, M. Tjoelker, and D. Tissue (2017), Stomatal and non-
 1125 stomatal limitations of photosynthesis for four tree species under drought: A compar-
 1126 ison of model formulations, *Agricultural and Forest Meteorology*, 247, 454 – 466, doi:
 1127 https://doi.org/10.1016/j.agrformet.2017.08.026.
- 1128 Egea, G., A. Verhoef, and P. L. Vidale (2011), Towards an improved and more flex-
 1129 ible representation of water stress in coupled photosynthesis-stomatal con-
 1130 ductance models, *Agricultural and Forest Meteorology*, 151(10), 1370 – 1384, doi:
 1131 https://doi.org/10.1016/j.agrformet.2011.05.019.
- 1132 Entekhabi, D., E. G. Njoku, P. E. O'Neill, K. H. Kellogg, W. T. Crow, W. N. Edelstein,
 1133 J. K. Entin, S. D. Goodman, T. J. Jackson, J. Johnson, J. Kimball, J. R. Piepmeier,
 1134 R. D. Koster, N. Martin, K. C. McDonald, M. Moghaddam, S. Moran, R. Reichle, J. C.
 1135 Shi, M. W. Spencer, S. W. Thurman, L. Tsang, and J. V. Zyl (2010), The soil mois-
 1136 ture active passive (smap) mission, *Proceedings of the IEEE*, 98(5), 704–716, doi:
 1137 10.1109/JPROC.2010.2043918.
- 1138 Epila, J., N. J. De Baerdemaeker, L. L. Vergeynst, W. H. Maes, H. Beeckman, and K. Steppe
 1139 (2017), Capacitive water release and internal leaf water relocation delay drought-
 1140 induced cavitation in African *Maesopsis eminii*, *Tree Physiology*, 37(4), 481–490, doi:
 1141 10.1093/treephys/tpw128.
- 1142 Farquhar, G. D., S. von Caemmerer, and J. A. Berry (1980), A biochemical model of
 1143 photosynthetic CO₂ assimilation in leaves of C₃ species, *Planta*, 149(1), 78–90, doi:
 1144 10.1007/BF00386231.
- 1145 Ficklin, D. L., and K. A. Novick (2017), Historic and projected changes in vapor pressure
 1146 deficit suggest a continental-scale drying of the United States atmosphere, *Journal of*
1147 Geophysical Research: Atmospheres, 122(4), 2061–2079, doi:10.1002/2016JD025855.
- 1148 Fisher, R. A., M. Williams, R. L. Do Vale, A. L. Da Costa, and P. Meir (2006), Evidence
 1149 from Amazonian forests is consistent with isohydric control of leaf water potential, *Plant*,
1150 Cell & Environment, 29(2), 151–165, doi:10.1111/j.1365-3040.2005.01407.x.

- Fisher, R. A., M. Williams, A. L. D. Costa, Y. Malhi, R. F. D. Costa, S. Almeida, and P. Meir (2007), The response of an Eastern Amazonian rain forest to drought stress: results and modelling analyses from a throughfall exclusion experiment, *Global Change Biology*, 13(11), 2361–2378, doi:10.1111/j.1365-2486.2007.01417.x.
- Fisher, R. A., M. Williams, M. de Lourdes Ruivo, A. L. de Costa, and P. Meir (2008), Evaluating climatic and soil water controls on evapotranspiration at two Amazonian rainforest sites, *Agricultural and Forest Meteorology*, 148(6), 850 – 861, doi: <https://doi.org/10.1016/j.agrformet.2007.12.001>.
- Flexas, J., J. Bota, F. Loreto, G. Cornic, and T. D. Sharkey (2004), Diffusive and metabolic limitations to photosynthesis under drought and salinity in c3 plants, *Plant Biology*, 6(3), 269–279, doi:10.1055/s-2004-820867.
- Flexas, J., M. Ribas-Carbó, J. Bota, J. Galmés, M. Henkle, S. Martínez-Cañellas, and H. Medrano (2006), Decreased rubisco activity during water stress is not induced by decreased relative water content but related to conditions of low stomatal conductance and chloroplast CO₂ concentration, *New Phytologist*, 172(1), 73–82, doi:10.1111/j.1469-8137.2006.01794.x.
- Franks, P. J., P. L. Drake, and R. H. Froend (2007), Anisohydric but isohydrodynamic: seasonally constant plant water potential gradient explained by a stomatal control mechanism incorporating variable plant hydraulic conductance, *Plant, Cell & Environment*, 30(1), 19–30, doi:10.1111/j.1365-3040.2006.01600.x.
- Friedlingstein, P., M. Meinshausen, V. K. Arora, C. D. Jones, A. Anav, S. K. Liddicoat, and R. Knutti (2014), Uncertainties in CMIP5 climate projections due to carbon cycle feedbacks, *Journal of Climate*, 27(2), 511–526.
- Fu, R., L. Yin, W. Li, P. A. Arias, R. E. Dickinson, L. Huang, S. Chakraborty, K. Fernandes, B. Liebmann, R. Fisher, and R. B. Myneni (2013), Increased dry-season length over southern Amazonia in recent decades and its implication for future climate projection, *Proceedings of the National Academy of Sciences of the United States of America*, 110(45), 18,110–18,115.
- Gentine, P., M. Guérin, M. Uriarte, N. G. McDowell, and W. T. Pockman (2016), An allometry-based model of the survival strategies of hydraulic failure and carbon starvation, *Ecohydrology*, 9(3), 529–546, doi:10.1002/eco.1654.
- Grant, J., J.-P. Wigneron, R. D. Jeu, H. Lawrence, A. Mialon, P. Richaume, A. A. Bitar, M. Drusch, M. van Marle, and Y. Kerr (2016), Comparison of SMOS and AMSR-E vegetation optical depth to four MODIS-based vegetation indices, *Remote Sensing of Environment*, 172, 87 – 100, doi:<https://doi.org/10.1016/j.rse.2015.10.021>.
- Green, J. K., A. G. Konings, S. H. Alemohammad, J. Berry, D. Entekhabi, J. Kolassa, J.-E. Lee, and P. Gentine (2017), Regionally strong feedbacks between the atmosphere and terrestrial biosphere, *Nature Geoscience*, 10(6), 410–414, doi:10.1038/ngeo2957.
- Harley, P. C., R. B. Thomas, J. F. Reynolds, and B. R. Strain (1992), Modelling photosynthesis of cotton grown in elevated co₂, *Plant Cell Environment*, 15(3), 271–282, doi: 10.1111/j.1365-3040.1992.tb00974.x.
- Holbrook, N. M., E. T. Ahrens, M. J. Burns, and M. A. Zwieniecki (2001), In vivo observation of cavitation and embolism repair using magnetic resonance imaging, *Plant Physiology*, 126(1), 27–31, doi:10.1104/pp.126.1.27.
- Jackson, R. B., J. Canadell, J. R. Ehleringer, H. A. Mooney, O. E. Sala, and E. D. Schulze (1996), A global analysis of root distributions for terrestrial biomes, *Oecologia*, 108(3), 389–411, doi:10.1007/BF00333714.
- Joetzjer, E., C. Delire, H. Douville, P. Ciais, B. Decharme, R. Fisher, B. Christoffersen, J. C. Calvet, A. C. L. da Costa, L. V. Ferreira, and P. Meir (2014), Predicting the response of the Amazon rainforest to persistent drought conditions under current and future climates: a major challenge for global land surface models, *Geoscientific Model Development*, 7(6), 2933–2950, doi:10.5194/gmd-7-2933-2014.
- Kattge, J., S. DÑAZ, S. Lavorel, I. C. Prentice, P. Leadley, G. BÑNisch, E. Garnier, M. Westoby, P. B. Reich, I. J. Wright, J. H. C. Cornelissen, C. Viole, S. P. Harri-

- son, P. M. Van Bodegom, M. ReichSTEIN, B. J. Enquist, N. A. Soudzilovskaia, D. D. Ackerly, M. Anand, O. Atkin, M. Bahn, T. R. Baker, D. Baldocchi, R. Bekker, C. C. Blanco, B. Blonder, W. J. Bond, R. Bradstock, D. E. Bunker, F. Casanoves, J. Cavender-Bares, J. Q. Chambers, F. S. Chapin III, J. Chave, D. Coomes, W. K. Cornwell, J. M. Craine, B. H. Dobrin, L. Duarte, W. Durka, J. Elser, G. Esser, M. Estiarte, W. F. Fagan, J. Fang, F. Fernández-MÁNDEZ, A. Fidelis, B. Finegan, O. Flores, H. Ford, D. Frank, G. T. Freschet, N. M. Fyllas, R. V. Gallagher, W. A. Green, A. G. Gutierrez, T. Hickler, S. I. Higgins, J. G. Hodgson, A. Jalili, S. Jansen, C. A. Joly, A. J. Kerkhoff, D. Kirkup, K. Kitajima, M. Kleyer, S. Klotz, J. M. H. Knops, K. Kramer, I. KAIJHN, H. Kurokawa, D. Laughlin, T. D. Lee, M. Leishman, F. Lens, T. Lenz, S. L. Lewis, J. Lloyd, J. Llusiá, F. Louault, S. Ma, M. D. MaHECHA, P. MaNNING, T. MaSSAD, B. E. Medlyn, J. Messier, A. T. Moles, S. C. MÁIJLLER, K. Nadrowski, S. Naeem, Á. Niinimets, S. NÄÜllerT, A. NÄIJSKE, R. Ogaya, J. Oleksyn, V. G. Onipchenko, Y. Onoda, J. OrdoñEZ, G. Overbeck, W. A. Ozinga, S. PatiÁO, S. Paula, J. G. Pausas, J. PeÁSUELAS, O. L. Phillips, V. Pillar, H. Poorter, L. Poorter, P. Poschlod, A. Prinzing, R. Proulx, A. Rammig, S. Reinsch, B. Reu, L. Sack, B. Salgado-Negret, J. Sardans, S. Shiodera, B. Shipley, A. Siefert, E. Sosinski, J.-F. Soussana, E. Swaine, N. Swenson, K. Thompson, P. Thornton, M. Waldram, E. Weiher, M. White, S. White, S. J. Wright, B. Yguel, S. Zahle, A. E. Zanne, and C. Wirth (2011), Try a global database of plant traits, *Global Change Biology*, 17(9), 2905–2935, doi:10.1111/j.1365-2486.2011.02451.x.
- Klein, T., and S. Niu (2014), The variability of stomatal sensitivity to leaf water potential across tree species indicates a continuum between isohydric and anisohydric behaviours, *Functional Ecology*, 28(6), 1313–1320, doi:10.1111/1365-2435.12289.
- Konings, A. G., and P. Gentine (2017a), Global variations in ecosystem-scale isohydricity, *Global Change Biology*, 23(2), 891–905, doi:10.1111/gcb.13389.
- Konings, A. G., M. Piles, K. RÄÜTZER, K. A. McColl, S. K. Chan, and D. Entekhabi (2016), Vegetation optical depth and scattering albedo retrieval using time series of dual-polarized l-band radiometer observations, *Remote Sensing of Environment*, 172, 178 – 189, doi: <https://doi.org/10.1016/j.rse.2015.11.009>.
- Konings, A. G., A. P. Williams, and P. Gentine (2017b), Sensitivity of grassland productivity to aridity controlled by stomatal and xylem regulation, *Nature Geoscience*, 10(4), 284–288, doi:10.1038/ngeo2903.
- Lee, J.-E., R. S. Oliveira, T. E. Dawson, and I. Fung (2005), Root functioning modifies seasonal climate, *Proceedings of the National Academy of Sciences of the United States of America*, 102(49), 17,576–17,581, doi:10.1073/pnas.0508785102.
- Lin, C., P. Gentine, Y. Huang, K. Guan, H. Kimm, and S. Zhou (2018), Diel ecosystem conductance response to vapor pressure deficit is suboptimal and independent of soil moisture, *Agricultural and Forest Meteorology*, 250-251, 24 – 34, doi: <https://doi.org/10.1016/j.agrformet.2017.12.078>.
- Mackay, D. S., D. E. Roberts, B. E. Ewers, J. S. Sperry, N. G. McDowell, and W. T. Pockman (2015), Interdependence of chronic hydraulic dysfunction and canopy processes can improve integrated models of tree response to drought, *Water Resources Research*, 51(8), 6156–6176, doi:10.1002/2015WR017244.
- Manzoni, S., G. Vico, G. Katul, P. A. Fay, W. Polley, S. Palmroth, and A. Porporato (2011), Optimizing stomatal conductance for maximum carbon gain under water stress: a meta-analysis across plant functional types and climates, *Functional Ecology*, 25(3), 456–467, doi:10.1111/j.1365-2435.2010.01822.x.
- Manzoni, S., G. Vico, S. Palmroth, A. Porporato, and G. Katul (2013a), Optimization of stomatal conductance for maximum carbon gain under dynamic soil moisture, *Advances in Water Resources*, 62, 90 – 105, doi:<https://doi.org/10.1016/j.advwatres.2013.09.020>.
- Manzoni, S., G. Vico, G. Katul, S. Palmroth, R. B. Jackson, and A. Porporato (2013b), Hydraulic limits on maximum plant transpiration and the emergence of the safety-efficiency trade-off, *New Phytologist*, 198(1), 169–178, doi:10.1111/nph.12126.

- 1260 McDowell, N. G., and C. D. Allen (2015), Darcy's law predicts widespread forest mortality
 1261 under climate warming, *Nature Climate Change*, 5(7), 669–672.
- 1262 McDowell, N. G., R. A. Fisher, C. Xu, J. C. Domec, T. HÃºlittÃ©, D. S. Mackay, J. S. Sperry,
 1263 A. Boutz, L. Dickman, N. Gehres, J. M. Limousin, A. Macalady, J. MartÃ¡nez-Vilalta,
 1264 M. Mencuccini, J. A. Plaut, J. OgÃ©e, R. E. Pangle, D. P. Rasse, M. G. Ryan, S. Sevanto,
 1265 R. H. Waring, A. P. Williams, E. A. Yepez, and W. T. Pockman (2013), Evaluating theories
 1266 of drought-induced vegetation mortality using a multimodel experiment framework,
 1267 *New Phytologist*, 200(2), 304–321, doi:10.1111/nph.12465.
- 1268 McDowell, N. G., A. P. Williams, C. Xu, W. T. Pockman, L. T. Dickman, S. Sevanto, R. Pan-
 1269 ggle, J. Limousin, J. Plaut, D. S. Mackay, J. Ogee, J. C. Domec, C. D. Allen, R. A. Fisher,
 1270 X. Jiang, J. D. Muss, D. D. Breshears, S. A. Rauscher, and C. Koven (2016), Multi-scale
 1271 predictions of massive conifer mortality due to chronic temperature rise, *Nature Climate
 1272 Change*, 6, 295–300, doi:10.1038/nclimate2873.
- 1273 Medlyn, B. E., R. A. Duursma, D. Eamus, D. S. Ellsworth, I. C. Prentice, C. V. M. Barton,
 1274 K. Y. Crous, P. De Angelis, M. Freeman, and L. Wingate (2011), Reconciling the optimal
 1275 and empirical approaches to modelling stomatal conductance, *Global Change Biology*,
 1276 17(6), 2134–2144, doi:10.1111/j.1365-2486.2010.02375.x.
- 1277 Meinzer, F. C., S. A. James, and G. Goldstein (2004), Dynamics of transpiration, sap flow
 1278 and use of stored water in tropical forest canopy trees, *Tree Physiology*, 24(8), 901–909,
 1279 doi:10.1093/treephys/24.8.901.
- 1280 Meinzer, F. C., D. M. Johnson, B. Lachenbruch, K. A. McCulloh, and D. R. Woodruff
 1281 (2009), Xylem hydraulic safety margins in woody plants: coordination of stomatal con-
 1282 trol of xylem tension with hydraulic capacitance, *Functional Ecology*, 23(5), 922–930,
 1283 doi:10.1111/j.1365-2435.2009.01577.x.
- 1284 Momen, M., J. D. Wood, K. A. Novick, R. Pangle, W. T. Pockman, N. G. McDowell, and
 1285 A. G. Konings (2017), Interacting effects of leaf water potential and biomass on vegetation
 1286 optical depth, *Journal of Geophysical Research: Biogeosciences*, 122(11), 3031–3046,
 1287 doi:10.1002/2017JG004145.
- 1288 Nepstad, D. C., R. de Carvalho, Claudio, E. A. Davidson, P. H. Jipp, and e. al (1994), The
 1289 role of deep roots in the hydrological and carbon cycles of amazonian forests and pastures,
 1290 *Nature*, 372(6507), 666.
- 1291 Novick, K. A., D. L. Ficklin, P. C. Stoy, C. A. Williams, G. Bohrer, A. Oishi, S. A. Papuga,
 1292 P. D. Blanken, A. Noormets, B. N. Sulman, R. L. Scott, L. Wang, and R. P. Phillips
 1293 (2016a), The increasing importance of atmospheric demand for ecosystem water and car-
 1294 bon fluxes, *Nature Climate Change*, 6(11), 1023–1027.
- 1295 Novick, K. A., C. F. Miniat, and J. M. Vose (2016b), Drought limitations to leaf-level gas
 1296 exchange: results from a model linking stomatal optimization and cohesion-tension theory,
 1297 *Plant, Cell & Environment*, 39(3), 583–596, doi:10.1111/pce.12657.
- 1298 Oleson, K. W., D. M. Lawrence, G. B. Bonan, B. Drewniak, M. Huang, C. D. Koven,
 1299 S. Levis, F. Li, W. J. Riley, Z. M. Subin, S. C. Swenson, P. E. Thornton, A. Bozbiyik,
 1300 R. Fisher, C. L. Heald, E. Kluzek, J.-F. Lamarque, P. J. Lawrence, L. R. Leung, W. Lip-
 1301 scomb, S. Muszala, D. M. Ricciuto, W. Sacks, Y. Sun, J. Tang, and Z.-L. Yang (2013),
 1302 Technical description of version 4.5 of the community land model (clm), NCAR Tech.
 1303 Note NCAR/TN-503+STR, *National Center for Atmospheric Research, Boulder, Col-
 1304 orado*, 420 pp., doi:10.5065/D6RR1W7M.
- 1305 Oliveira, R. S., T. E. Dawson, S. S. O. Burgess, and D. C. Nepstad (2005), Hydraulic redis-
 1306 tribution in three amazonian trees, *Oecologia*, 145(3), 354–363, doi:10.1007/s00442-005-
 1307 0108-2.
- 1308 Powell, T. L., D. R. Galbraith, B. O. Christoffersen, A. Harper, H. M. A. Imbuzeiro, L. Row-
 1309 land, S. Almeida, P. M. Brando, A. C. L. da Costa, M. H. Costa, N. M. Levine, Y. Malhi,
 1310 S. R. Saleska, E. Sotta, M. Williams, P. Meir, and P. R. Moorcroft (2013), Confronting
 1311 model predictions of carbon fluxes with measurements of amazon forests subjected to ex-
 1312 perimental drought, *New Phytologist*, 200(2), 350–365, doi:10.1111/nph.12390.

- 1313 Restaino, C. M., D. L. Peterson, and J. Littell (2016), Increased water deficit decreases dou-
 1314 glas fir growth throughout western US forests, *Proceedings of the National Academy of*
 1315 *Sciences*, 113(34), 9557–9562, doi:10.1073/pnas.1602384113.
- 1316 Restrepo-Coupe, N., N. M. Levine, B. O. Christoffersen, L. P. Albert, J. Wu, M. H. Costa,
 1317 D. Galbraith, H. Imbuzeiro, G. Martins, A. C. da Araujo, Y. S. Malhi, X. Zeng, P. Moor-
 1318 croft, and S. R. Saleska (2017), Do dynamic global vegetation models capture the season-
 1319 ality of carbon fluxes in the amazon basin? A data-model intercomparison, *Global Change*
 1320 *Biology*, 23(1), 191–208, doi:10.1111/gcb.13442.
- 1321 Sack, L., P. J. Melcher, M. A. Zwieniecki, and N. M. Holbrook (2002), The hydraulic con-
 1322 ductance of the angiosperm leaf lamina: a comparison of three measurement methods,
 1323 *Journal of Experimental Botany*, 53(378), 2177–2184.
- 1324 Scholz, F. G., N. G. Phillips, S. J. Bucci, F. C. Meinzer, and G. Goldstein (2011), Hydraulic
 1325 capacitance: Biophysics and functional significance of internal water sources, in Meinzer,
 1326 F.C., Lachenbruch, B., Dawson, T. E. (eds) *Size- and Age-Related Changes in Tree Struc-*
 1327 *ture and Function*, pp. 341–361, Springer, Dordrecht.
- 1328 Seager, R., A. Hooks, A. P. Williams, B. Cook, J. Nakamura, and N. Henderson (2015), Cli-
 1329 matology, variability, and trends in the u.s. vapor pressure deficit, an important fire-related
 1330 meteorological quantity, *Journal of Applied Meteorology and Climatology*, 54(6), 1121–
 1331 1141, doi:10.1175/JAMC-D-14-0321.1.
- 1332 Sellers, P. J., D. A. Randall, G. J. Collatz, J. A. Berry, C. B. Field, D. A. Dazlich, C. Zhang,
 1333 G. D. Collelo, and L. Bounoua (1996a), a revised land surface parameterization (sib2)
 1334 for atmospheric gcms. part i: Model formulation, *Journal of Climate*, 9(4), 676–705, doi:
 1335 10.1175/1520-0442(1996)009<0676:ARLSPF>2.0.CO;2.
- 1336 Sellers, P. J., C. J. Tucker, G. J. Collatz, S. O. Los, C. O. Justice, D. A. Dazlich, and
 1337 D. A. Randall (1996b), A revised land surface parameterization (sib2) for atmo-
 1338 spheric gcms. part ii: The generation of global fields of terrestrial biophysical pa-
 1339 rameters from satellite data, *Journal of Climate*, 9(4), 706–737, doi:10.1175/1520-
 1340 0442(1996)009<0706:ARLSPF>2.0.CO;2.
- 1341 Sheffield, J., E. F. Wood, and M. L. Roderick (2012), Little change in global drought over the
 1342 past 60 years, *Nature*, 491(7424), 435–8.
- 1343 Simonin, K. A., E. Burns, B. Choat, M. M. Barbour, T. E. Dawson, and P. J. Franks (2015),
 1344 Increasing leaf hydraulic conductance with transpiration rate minimizes the water potential
 1345 drawdown from stem to leaf, *Journal of Experimental Botany*, 66(5), 1303–1315, doi:
 1346 10.1093/jxb/eru481.
- 1347 Siqueira, M., G. Katul, and A. Porporato (2008), Onset of water stress, hysteresis in plant
 1348 conductance, and hydraulic lift: Scaling soil water dynamics from millimeters to meters,
 1349 *Water Resources Research*, 44(1), W01,432, doi:10.1029/2007WR006094.
- 1350 Sperry, J. S., and D. M. Love (2015), What plant hydraulics can tell us about responses to
 1351 climate-change droughts, *New Phytologist*, 207(1), 14–27, doi:10.1111/nph.13354.
- 1352 Sperry, J. S., F. R. Adler, G. S. Campbell, and J. P. Comstock (1998), Limitation of plant
 1353 water use by rhizosphere and xylem conductance: results from a model, *Plant Cell Envi-*
 1354 *ronment*, 21(4), 347–359, doi:10.1046/j.1365-3040.1998.00287.x.
- 1355 Sperry, J. S., U. G. Hacke, R. Oren, and J. P. Comstock (2002), Water deficits and hy-
 1356 draulic limits to leaf water supply, *Plant, Cell & Environment*, 25(2), 251–263, doi:
 1357 10.1046/j.0016-8025.2001.00799.x.
- 1358 Sperry, J. S., M. D. Venturas, W. R. L. Anderegg, M. Mencuccini, D. S. Mackay, Y. Wang,
 1359 and D. M. Love (2017), Predicting stomatal responses to the environment from the op-
 1360 timization of photosynthetic gain and hydraulic cost, *Plant, Cell & Environment*, 40(6),
 1361 816–830, doi:10.1111/pce.12852, pCE-16-0541.R1.
- 1362 Thornton, P. E., and N. E. Zimmermann (2007), An improved canopy integration scheme for
 1363 a land surface model with prognostic canopy structure, *Journal of Climate*, 20(15), 3902–
 1364 3923, doi:10.1175/JCLI4222.1.
- 1365 Tyree, M. T., and J. S. Sperry (1988), Do woody plants operate near the point of catastrophic
 1366 xylem dysfunction caused by dynamic water stress?: Answers from a model, *Plant Physi-*

- 1367 *ology*, 88(3), 574–580.
- 1368 Tyree, M. T., and J. S. Sperry (1989), Vulnerability of xylem to cavitation and embolism,
1369 *Annual Review of Plant Physiology and Plant Molecular Biology*, 40(1), 19–36, doi:
1370 10.1146/annurev.pp.40.060189.000315.
- 1371 Ukkola, A. M., M. G. D. Kauwe, A. J. Pitman, M. J. Best, G. Abramowitz, V. Haverd,
1372 M. Decker, and N. Haughton (2016), Land surface models systematically overestimate the
1373 intensity, duration and magnitude of seasonal-scale evaporative droughts, *Environmental
1374 Research Letters*, 11(10), 104,012.
- 1375 Verhoef, A., and G. Egea (2014), Modeling plant transpiration under limited soil water:
1376 Comparison of different plant and soil hydraulic parameterizations and preliminary im-
1377 plications for their use in land surface models, *Agricultural and Forest Meteorology*, 191,
1378 22–32, doi:<https://doi.org/10.1016/j.agrformet.2014.02.009>.
- 1379 Williams, A. P., C. D. Allen, A. K. Macalady, D. Griffin, C. A. Woodhouse, D. M. Meko,
1380 T. W. Swetnam, S. A. Rauscher, R. Seager, H. Grissino-Mayer, J. S. Dean, E. R. Cook,
1381 C. Gangodagamage, M. Cai, and N. G. McDowell (2013), Temperature as a potent driver
1382 of regional forest drought stress and tree mortality, *Nature Climate Change*, 3(3), 292–297.
- 1383 Williams, M., E. B. Rastetter, D. N. Fernandes, M. L. Goulden, S. C. Wofsy, G. R. Shaver,
1384 J. M. Melillo, J. W. Munger, S.-M. Fan, and K. J. Nadelhoffer (1996), Modelling the soil-
1385 plant-atmosphere continuum in a *quercus* stand at harvard forest: the regulation of
1386 stomatal conductance by light, nitrogen and soil/plant hydraulic properties, *Plant, Cell &
1387 Environment*, 19(8), 911–927, doi:10.1111/j.1365-3040.1996.tb00456.x.
- 1388 Williams, M., B. E. Law, P. M. Anthoni, and M. H. Unsworth (2001), Use of a simulation
1389 model and ecosystem flux data to examine carbon–water interactions in ponderosa
1390 pine., *Tree Physiology*, 21(5), 287 – 298.
- 1391 Xu, X., D. Medvigy, J. S. Powers, J. M. Becknell, and K. Guan (2016), Diversity in plant
1392 hydraulic traits explains seasonal and inter-annual variations of vegetation dynamics in
1393 seasonally dry tropical forests, *New Phytologist*, 212(1), 80–95, doi:10.1111/nph.14009,
1394 2015-20772.
- 1395 Zhou, S., R. A. Duursma, B. E. Medlyn, J. W. Kelly, and I. C. Prentice (2013), How should
1396 we model plant responses to drought? An analysis of stomatal and non-stomatal re-
1397 sponses to water stress, *Agricultural and Forest Meteorology*, 182-183, 204 – 214, doi:
1398 <https://doi.org/10.1016/j.agrformet.2013.05.009>.
- 1399 Zhou, S., B. Medlyn, S. Sabaté, D. Sperlich, I. C. Prentice, and D. Whitehead (2014), Short-
1400 term water stress impacts on stomatal, mesophyll and biochemical limitations to photosyn-
1401 thesis differ consistently among tree species from contrasting climates, *Tree Physiology*,
1402 34(10), 1035, doi:10.1093/treephys/tpu072.